RECLAMATION
Managing Water in the West

Technical Memorandum No. MERL-2012-10

Electro-Osmotic Pulse Leak Repair Method: Evaluation in Trinity Dam Bonnet Chamber

U.S. Department of the Interior
Bureau of Reclamation

May 2012

Mission Statements

The U.S. Department of the Interior protects America's natural resources and heritage, honors our cultures and tribal communities, and supplies the energy to power our future.

The mission of the Bureau of Reclamation is to manage, develop, and protect water and related resources in an environmentally and economically sound manner in the interest of the American public.
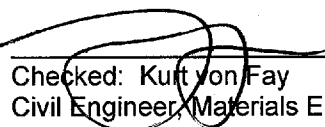
BUREAU OF RECLAMATION
Technical Service Center, Denver, Colorado
Materials Engineering and Research Lab Group, 86-68180

Technical Memorandum No. MERL-2012-10

Electro-Osmotic Pulse Leak Repair Method: Evaluation in Trinity Dam Bonnet Chamber
Central Valley Project, Trinity River Division – California
Trinity Dam, Mid-Pacific Region

Prepared: Daryl A. Little
Materials Engineer, Materials Engineering & Research Lab Group, 86-68180

5/16/12
Date

Checked: Kurt von Fay
Civil Engineer, Materials Engineering & Research Lab Group, 86-68180

5/17/12
Date

Editorial Approval: Teri Manross
Technical Writer-Editor, Client Support & Technical Presentations Office, 86-68010

5/17/12
Date

Technical Approval: Kurt von Fay
Civil Engineer, Materials Engineering & Research Lab Group, 86-68180

5/17/12
Date

Peer Review: William F. Kepler, P.E.
Civil Engineer, Materials Engineering & Research Lab Group, 86-68180

5/17/12
Date

REVISIONS					
Date	Description	Prepared	Checked	Technical Approval	Peer Review

Contents

Chapter I

Overview of the EOP Repair Method

Introduction

Electro-Osmotic Pulse (EOP) is a technology that uses current and electric fields to prevent water from leaking through concrete. It is potentially a long lasting solution to water intrusion through concrete. Results from previous installations performed by the U.S. Army Corps of Engineers show it has a lower life-cycle cost when compared to grouting or concrete repair alone.

The following are potential benefits of installing an EOP system to dry out a concrete structure:

1. New cracks within the EOP zone of influence do not compromise the system

2. Performance monitored "24-7"

3. Lower cost
   a. Negative side installation (buried or submerged side)
   b. Nondegradable, extremely durable
   c. Minimal maintenance
   d. Avoids costs of disruption and lost productivity

4. Highest return
   a. Prevents structural degradation of rebar from water penetrations

Because of EOP's potential to stop water leaks through concrete, a research program was initiated to test the technology at a Bureau of Reclamation (Reclamation) facility.

This report describes Phase 2 of a research effort to determine the applicability to Reclamation facilities. It also proposes a Phase 3 effort if results from Phase 2 are promising. Phase 1 consisted of a feasibility study involving site inspections, initial calculations, and project execution planning.

For Phase 2, EOP was installed in a small area of the gate chamber at Trinity Dam that was leaking water which was damaging equipment. This test area was selected to evaluate EOP on a small scale to determine if a larger scale test would be appropriate.

Conclusion

The EOP pilot test is operating as designed and has significantly reduced the moisture content of the concrete in the test area. This is based on the trend in the collected data that shows the resistance has increased over time at a constant voltage and the total current has decreased. Resistance of the concrete is directly related to the moisture content where the more moisture in the concrete the less resistance there is to current passed between the anode and cathode.

The success of the pilot test indicates that this technology does work in this type of application. However, the test section was small. A larger installation should be tested to more fully evaluate the technology. For the larger test section, EOP should be installed in the bottom 10 feet of the shaft, around its entire circumference. For this test, leaking cracks would be included in the test section. If the technology works for this larger test, it would likely work for the entire area of the gate shaft.

The technology may have application at a number of other Reclamation structures as well.

Test Location

Trinity Dam is near Redding, California, and was chosen as the site for the pilot test. The facility is experiencing water leaks through the bonnet chamber shaft, which leads to several maintenance problems in the shaft and bonnet chamber.

The walls of the shaft and bonnet chamber are covered with calcite as shown in figures 1a-1h. Calcite forms when water containing calcium ions reacts with carbon dioxide to form calcium carbonate. In some areas, the seepage over time has resulted in stalactite formation. The calcite has an average deposit thickness of 0.5 to 1 inch as shown in figures 2a-2d. Calcite has been measured as thick as 6 inches in the location shown in figures 1b and 1c. Due to the seepage, there is approximately 1 to 2 inches of standing water in some locations on the bonnet chamber floor, and corrosion of the air inlet pipe and bonnet cover has occurred, as shown in figures 3a-3d. The extent of the calcite deposits is preventing the operation of the door to the chamber as shown in figures 4a and 4b. If the door cannot be sealed, and the gate and bonnet cover fails, then water directly from the reservoir will flow through the door, down into the penstock tunnel, and then out into the powerplant yard.
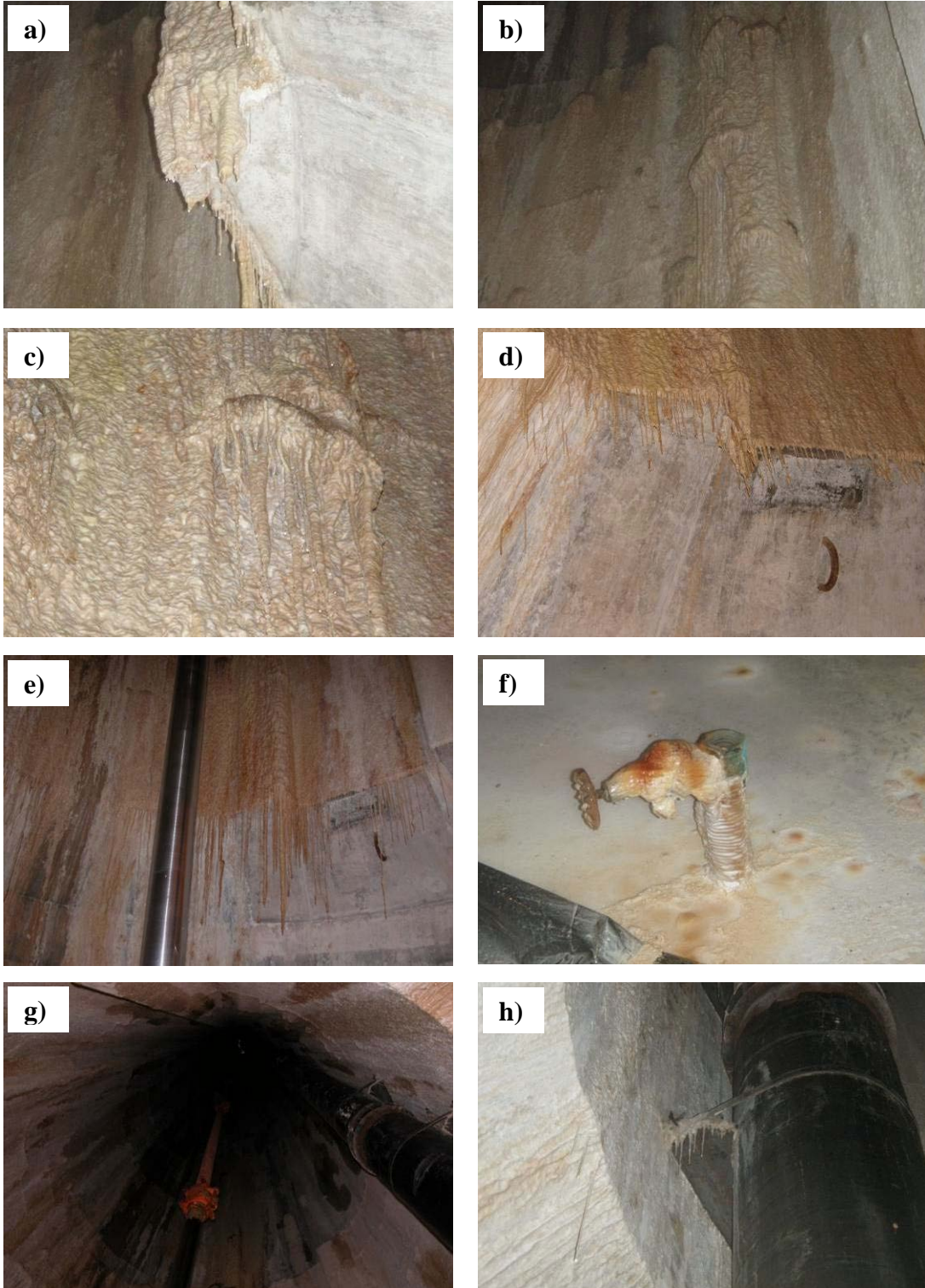
**Figure 1. Calcite deposits observed on the walls of the bonnet chamber.
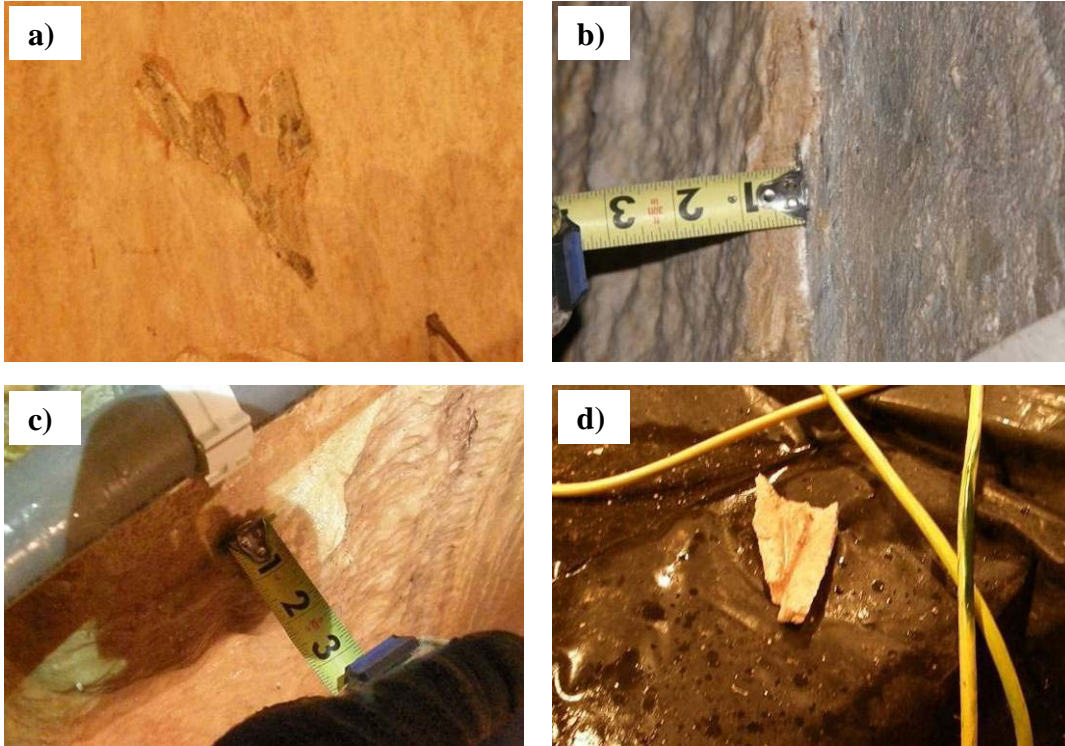Excessive seepage over time has resulted in stalactites and encasement of valves.**

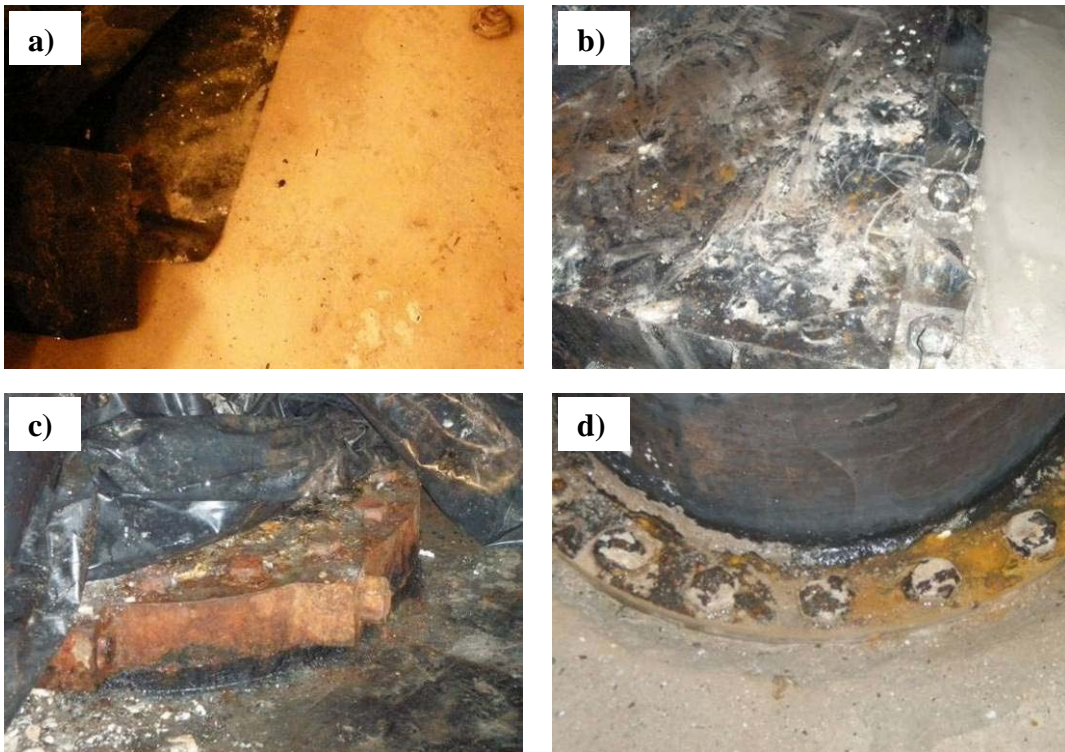**Figure 2. Calcite from the walls indicates an average thickness of 0.5 to 1 inch.**

Figure 3. Standing water from the seepage has caused corrosion of the air inlet pipe and bonnet cover.
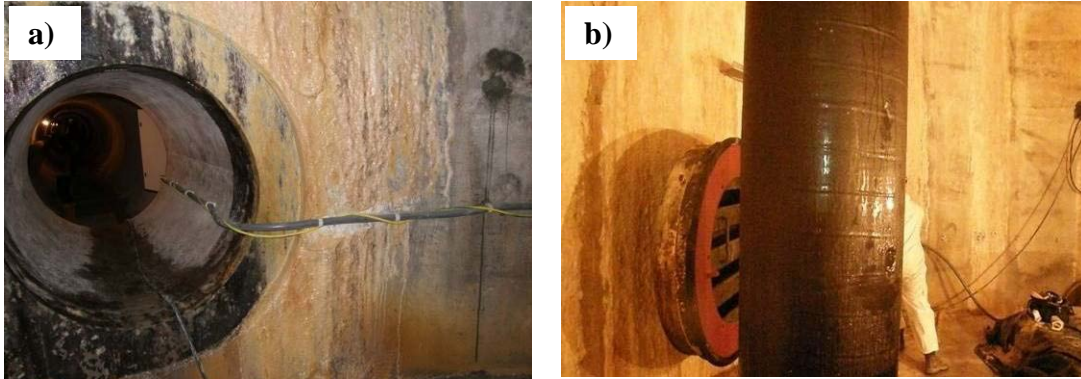
Figure 4. Excessive calcite deposit prevents the access door to the chamber from closing and sealing, creating an unsafe condition if the gate fails.

Objective and Approach

The objective of the second phase was to install EOP in a section of the bonnet chamber at Trinity Dam and monitor the EOP system performance in stopping water migration through the concrete at that location. The test section was a wall section approximately 14-foot-wide by 6 ½-foot-high located opposite the personnel entry tunnel. Figure 5 shows a schematic diagram of the installed system.

Figure 5. Schematic of installed system.

If measurements determine that the second phase is working, by drying out the concrete, then a recommendation will be made to install EOP in a larger test area. We currently envision using performance data to develop an exp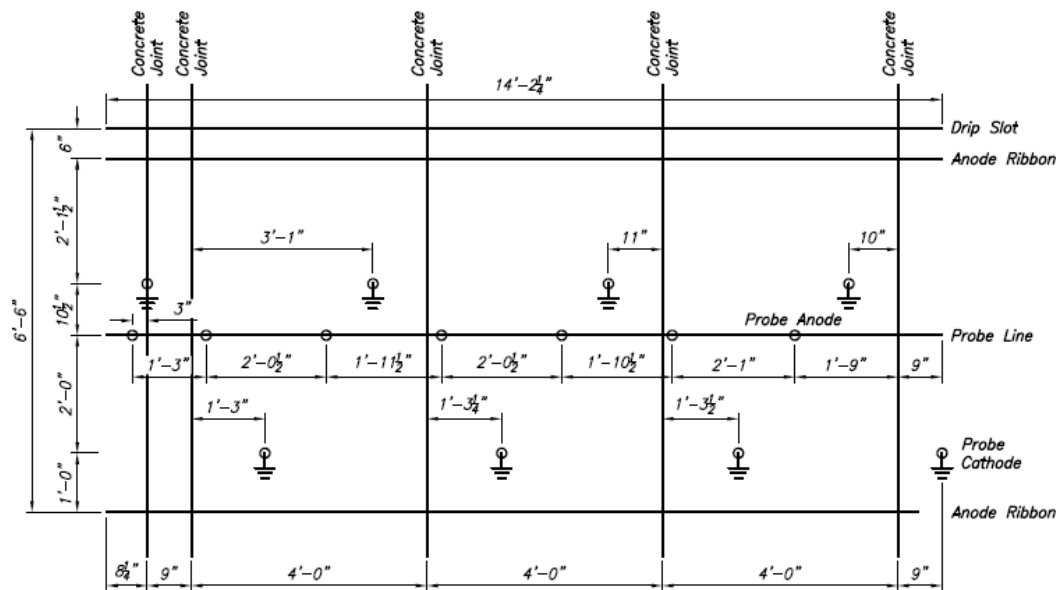anded test area for an EOP system to address water intrusion through a 10 foot high section at the bottom of the gate shaft above the bonnet chamber around the entire circumference. The next phase test section will include concrete that contains leaking cracks.

Background

Damage caused by water seeping through concrete or leaks through cracks in a concrete structure can be extensive and expensive to repair. Figure 6 shows sources of water in concrete structures. Corrosion of equipment inside the structure due to the resultant damp environment affects the operation of the equipment (e.g., gate operating motors and pipelines). Maintenance is required to mitigate the corrosion damage to the equipment, remove calcite deposits, and mitigate safety issues due to inoperable equipment and poor air quality. EOP technology can mitigate many water-related problems from the interior of affected areas without the cost of excavation. Corrosion and water/moisture related damage to equipment can be mitigated along with reducing humidity.
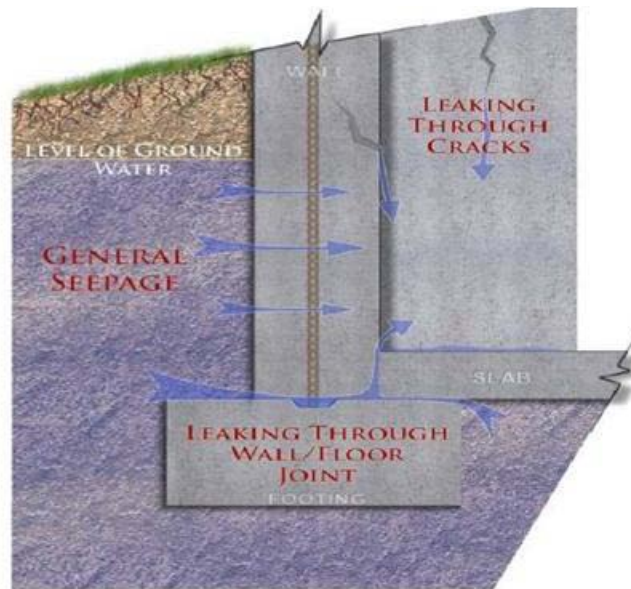
Figure 6. Sources of water and seepage [1, 2].

An EOP system involves inserting anodes (positive electrodes) into the concrete wall or floor on the inside of the structure and placing cathodes (negative electrodes) in the soil directly outside the structure. In the case of thick concrete walls or accessibility issues, the cathodes can be inserted into the wall to a given depth. Initial resistivity tests of the concrete and soil are utilized to determine the density of the anode and cathode placement. Figure 7 shows a typical EOP

system layout and operation. EOP systems require a 120-volt alternating current (V_{AC}) circuit for the system controller. The total power requirement for a 2,000-square-foot (ft^2) basement is about the same as that for a 100-watt incandescent light bulb [3].

Figure 7. Typical EOP system layout and operation [1, 2].

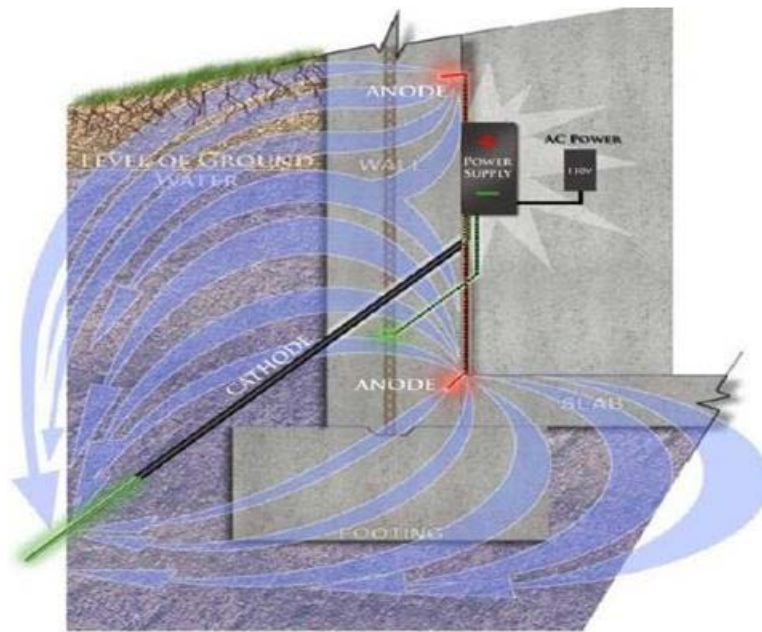## Concrete Chemistry and Structure

The primary "free" cations found in hydrated Portland cement are calcium, potassium, and sodium [4-6]. Roughly 90 percent of the total weight of hydrated cement paste consists of the following four products:

1. Tricalcium Silicate $3CaO.SiO_2$
2. Dicalcium Silicate $2CaO.SiO_2$
3. Tricalcium Aluminate $3CaO.Al_2O_3$
4. Tetracalcium Aluminoferrite $4CaO.Al_2O_3.Fe_2O_3$

Chemical shorthand for these compounds is as follows: $A = Al_2O_3$, $C = CaO$, $CH = Ca(OH)_2$, $F = Fe_2O_3$, $H = H_2O$, $S = SiO_2$, and $\overline{S} = SO_4$. If there are 2CaO molecules, it is expressed as C_2. The Portland cement phase hydration reactions are shown below by equations (1) through (6); however, these simple equations are not representative of the complexities of the reactions [4].
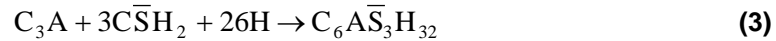
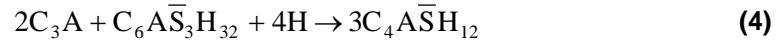Tricalcium Silicate + Water = Calcium Silicate Hydrate + Calcium Hydroxide

$$2C_3S + 11H \rightarrow C_3S_2H_8 + 3CH \tag{1}$$

Dicalcium Silicate + Water = Calcium Silicate Hydrate + Calcium Hydroxide

$$2C_2S + 9H \rightarrow C_3S_2H_8 + CH \qquad \qquad (2)$$

Tricalcium Aluminate + Gypsum + Water = Ettringite (Calcium Trisulfoaluminate Hydrate)

$$C_3A + 3C\overline{S}H_2 + 26H \rightarrow C_6A\overline{S}_3H_{32} \qquad \qquad (3)$$

Tricalcium Aluminate + Ettringite + Water = Calcium Monosulfoaluminate

$$2C_3A + C_6A\overline{S}_3H_{32} + 4H \rightarrow 3C_4A\overline{S}H_{12} \qquad \qquad (4)$$

Tricalcium Aluminate + Calcium Hydroxide + Water = Tetracalcium Aluminate Hydrate

$$C_3A + CH + 12H \rightarrow C_4AH_{13} \qquad \qquad (5)$$

Tetracalcium Aluminoferrite + Calcium Hydroxide + Water = Calcium Aluminoferrite Hydrate

$$C_4AF + 2CH + 10H \rightarrow C_6AFH_{12} \qquad \qquad (6)$$
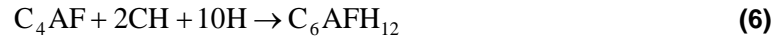
Cement paste microstructure is basically comprised of three "phases" as shown in figure 8 [7]. The hydrated cement particles are made up of a high-density calcium silicate hydrate (C-S-H) gel and act as solid particles in a continuous matrix comparable to aggregate particles [7]. The outer hydration product is the continuous phase in the capillary pore space and consists of solid C-S-H gel, gel pores, calcium hydroxide, and calcium sulfoaluminate phases [7].

Figure 8. Scanning electron microscope image of cement paste indicating main microstructural components [7].
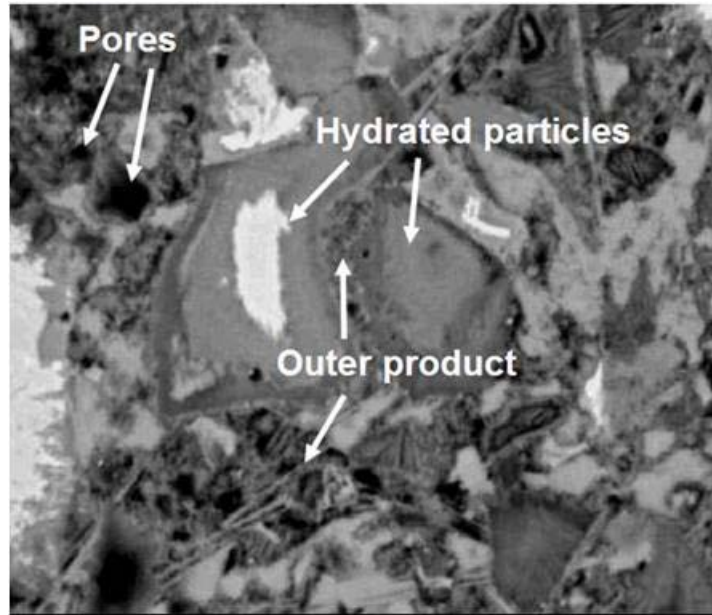
Large pores consist of true capillary pores, entrapped air voids, and the entrained air system and can be continuous or discontinuous, depending on the degree of hydration and starting water to cement ratio [7]. The relative volume of pores decreases with both time and degree of hydration as shown in figures 9 and 10, respectively. However, water is present in a variety of locations and different types of pores. The classifications of pores and features in concrete are capillary pore, gel pore, interlayer space, interfacial transition zone (ITZ) between cement paste and aggregate in the concrete, and microcracks. These features are identified in table 1, along with the size and type of water. The resultant phases from the hydration reactions replace the space in the cement occupied by water; however, if the water to cement ratio is larger than 0.35, porosity will still be present in the hardened cement and is called capillary porosity [4]. Therefore, the permeability and diffusivity transport properties increase with the increase in water to cement ratio due to the increasing porosity [4]. The increased transport properties can lead to degradation of the cement due to the ability of oxygen and water and, in some instances, chemicals to be transported to the reinforcing steel, leading to increased corrosion rates.
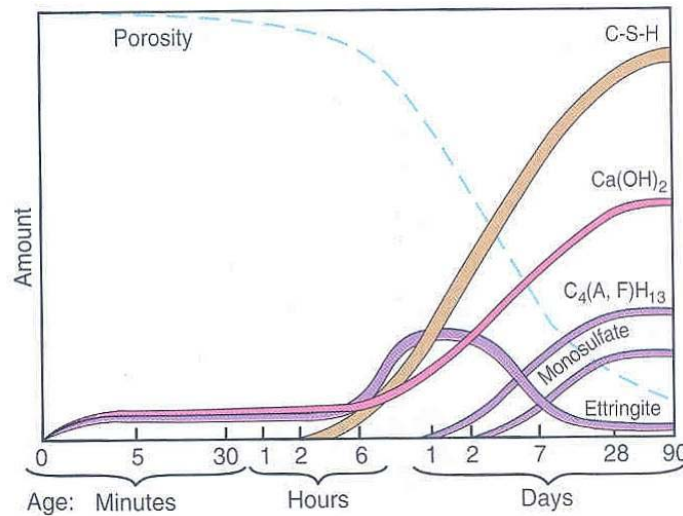
Figure 9. Relative volumes of phases and hydration products in hydrating Portland cement paste as a function of time [4].

Water in the cementitious materials exists in various forms such as free water and bound water. Free water includes the mixing water not yet reacted, and bound water is the water combined in the solid phases or physically bound to the solid surfaces [4]. The separation between the combined water from the physically adsorbed water is not reliably possible, and accordingly, Powers [8] distinguished between evaporable and nonevaporable water. All nonevaporable water is bound water, yet not all bound water is nonevaporable. A water to cement ratio of 0.4 is required for complete hydration of Portland cement; however, ratios greater than that will result in excess water, which, as previously stated, remains in the capillary pores or evaporates [4].
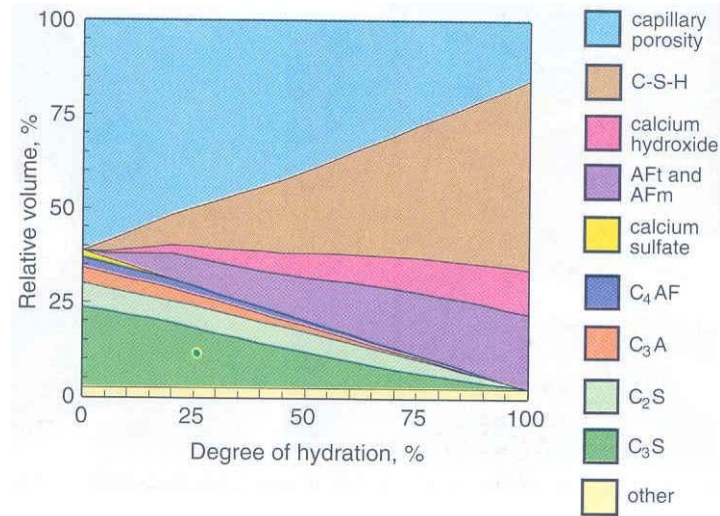
Figure 10. Relative volumes of phases and hydration products in hydrating Portland cement paste as a function of the degree of hydration as determined from a computer model for a water to cement ratio of 0.5 [4].

Table 1. Pore and feature classification in concrete [7]

Type of Pore	Description	Size	Water
Capillary pores	Large	10 μm – 50 nm	Evaporable bulk water
	Medium	50 – 10 nm	Evaporable moderate menisci
Gel pores	Small	10 – 2.5 nm	Evaporable strong menisci
	Micropores	2.5 – 0.5 nm	Nonevaporable, no menisci, intermolecular reactions
Interlayer spaces	Structural	< 0.5 nm	Nonevaporable, ionic/covalent bond
Other features	ITZ	20 – 50 μm	Bulk water
	Microcracks	50 - > 200 μm	Bulk water

Note: μm = micrometers (10^{-6} m), nm = nanometers (10^{-9} m)

In order to understand the condition and properties of concrete, it is essential to understand the rate of drying. Figure 11 shows the concrete drying rates for the three stages. Enough moisture is required throughout the curing period to achieve the desired properties and hydration. If the water to cement ratio is too low, moisture must come from an external source. During the first stage of drying, water is at the surface and evaporates into the air around the concrete if the humidity is low enough (figure 12) [9]. Temperature, relative humidity, and airflow over the surface control the rate of evaporation. Water within the body of the concrete replaces the evaporated water, which causes shrinkage of the concrete to maintain the volume [9]. If this rate is too high, the shrinkage is too excessive and will cause plastic shrinkage cracking early in the drying

process [9]. This is the primary cause of cracking, and the width of cracks is a function of the degree of drying, spacing or frequency of cracks, and the age at which the cracks occur [9].

Figure 11. The drying rate trends for the three stages of the drying of concrete. The rate of the first stage depends mostly on temperature, relative humidity, and air flow and is fairly constant. The rates of the second and third stages are more dependent on the cement paste [4].
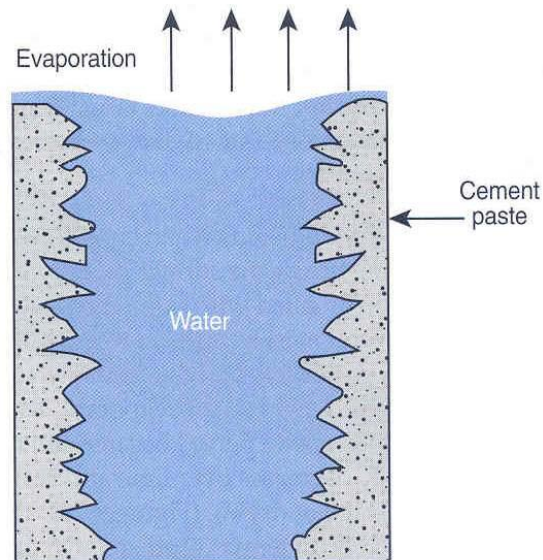

Figure 12. Drying stage 1: Pores in freshly placed concrete (or concrete that has been rewetted) are saturated with liquid water, and drying begins by evaporation from exposed surface [9].

The second stage of drying, shown in figure 13, initiates when the concrete can no longer shrink to accommodate the volume lost. Water from the surface recedes into the pores and clings to the walls to form a meniscus [9]. Water from the meniscus of the pores near the surface continues to evaporate into the air surrounding the concrete and, hence, is still dependent on the temperature, relative humidity, and air flow [9]. There is a steady decrease in the rate of drying during the second stage of the drying process as shown in figure 11.
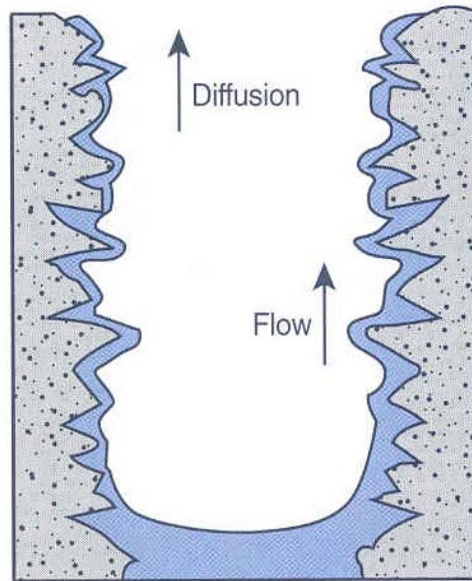

Figure 13. Drying stage 2: when moisture has retreated below the surface, movement depends on fluid flow along the surface of pores and evaporation into the pores [9].

The third stage of drying, called the second falling rate period, begins when the pores are no longer continuously filled with water due to evaporation as shown in figure 14 [9]. During this stage, the rate of drying continuously decreases over time and is slower than the previous stage of drying, as was shown in figure 11. Pockets of water still exist; however, moisture must now move by vapor diffusion within the concrete [9]. During this stage, the rate is more dependent on the quality of the cement paste than the factors which influence the rate of the first stage of drying [9]. The resistance to water vapor diffusion decreases as the water to cement ratio of the cement paste increases [9]. A continuously connected capillary pore system will take place when the water to cement ratio is sufficiently high and, therefore, the water vapor diffuse can more easily occur [9].
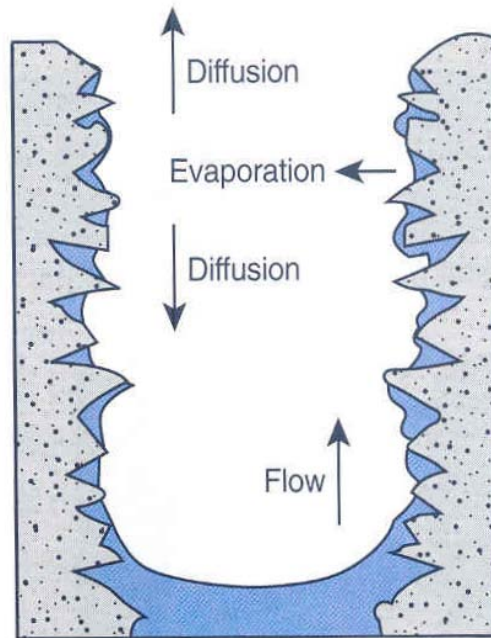
Figure 14. Drying stage 3: when moisture is no longer continuously wetting the surface of pores, moisture must evaporate within the body of the paste and diffuse toward the surface [9].

The concrete must be watertight or have a low permeability if the structure is water retaining, exposed to weather, or to other such exposure conditions. Water tightness is defined as the ability to hold back water without visible leakage, while permeability refers to the amount of water migration or the ability of concrete to resist water penetration. Four factors affect the permeability of concrete: (1) permeability of the paste; (2) permeability and gradation of the aggregate; (3) quality of the paste and aggregate transition zone; and (4) relative proportion of paste to aggregate [4]. The permeability of the paste is related to water to cement ratio, degree of cement hydration, and length of moist curing [4]. Low water to cement ratio and an adequate moist curing period yield a low permeable concrete. The water tightness of concrete increases with air entrapment but has little effect on the permeability; however, drying does increase the permeability [4]. Figure 15 shows test results obtained on thick non-air-entrained mortar disks [10]. The water leakage rate increased as the water to cement ratio was increased, but the water leakage rate decreased as the length of the moist curing time increased. The results show that low water to cement ratio and reasonable period of moist curing can significantly reduce the permeability of the concrete.
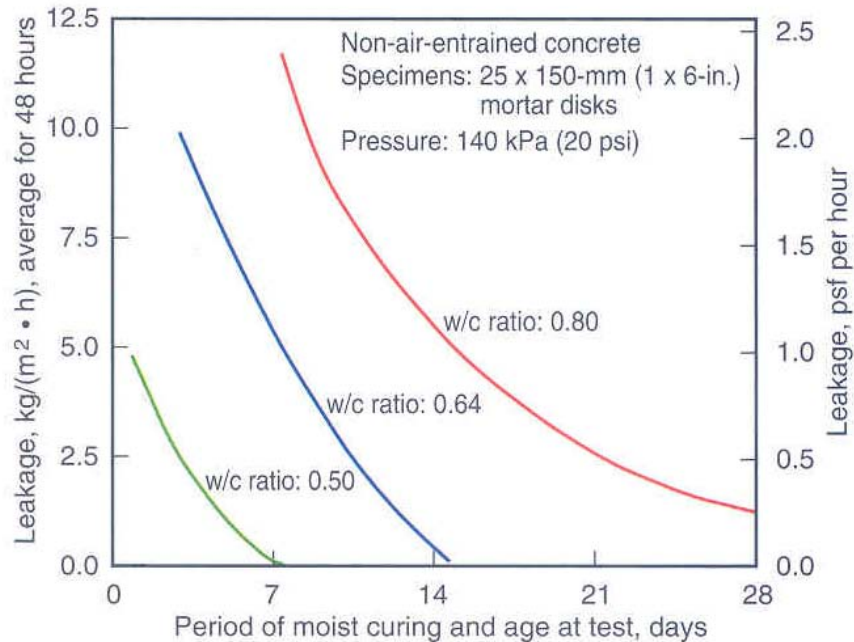
Figure 15. Effect of water to cement ratio and curing duration on permeability of mortar. Note that leakage is reduced as the water to cement ratio is decreased and the curing period is increased [10].

Principles of Electro-Osmotic Pulse Operation

An experiment conducted by F.F. Reuss in 1809 [11] showed that when an electric field was applied to the soil, water could be forced to flow through a clay-water system. Flow is initiated using the movement of positively charged ions (cations) in the pore fluid within a porous media like clay or concrete. The water surrounding the cations moves with them. This process is defined as electro-osmosis. The basic physics and chemistry of electro osmosis can be found in several textbooks and treatises [12-14]. Electro osmotic systems for waterproofing masonry walls were introduced in the 1960s by the Europeans [15].

The basic equation for the movement of the solution in concrete with a capillary pore system, as described by Tikhomolova [14], contains several forces as shown in equation 7 (sum of equations 7a to 7e). The terms on the right side of equation 7 are associated with the various force components. These force components include: the force due to gravity (equation 7a), the force due to pressure (equation 7b), the component due to viscosity (equation 7c), the electro-osmotic force (equation 7d), and the temperature component (equation 7e).

$$\rho \frac{d\vec{v}}{dt} = \overline{g}\rho \qquad \textbf{(7a)}$$

$$- grad\, p \tag{7b}$$

$$+ \eta \nabla^2 \vec{v}^0 \tag{7c}$$

$$+ \left(\frac{\rho^+ z^+ e_0}{m^+} + \frac{\rho^- z^- e_0}{m^-} \right) \vec{E} \tag{7d}$$

$$- \frac{kT}{m^+} grad\, \rho^+ - \frac{kT}{m^-} grad\, \rho^- \tag{7e}$$

Where:

ρ = density of solution

$\rho^{\pm}$ = density of the medium of the positive (negative) ions

$\vec{v}$ = velocity of the solution (center of mass)

$\vec{v}^0$ = velocity of the solvent

$\bar{g}$ = acceleration of gravity

p = pressure

η = shear viscosity coefficient

$z^{\pm}$ = charge of an ion

e_0 = elementary electric charge

$m^{\pm}$ = mass of a positive (negative) ion

$\vec{E}$ = strength of the electric field of the system

k = Boltzman constant

T = temperature

The forces due to pressure and electro-osmosis are generally the more dominant components, and to prevent water seepage caused by hydrostatic pressure, the force due to electro-osmosis must balance or exceed the pressure force [14]. The suitability and effectiveness of electro-osmosis is dependent on the presence of capillary pores, the concrete having fixed surface charges, saturation of the structure, and the solution in the pores must be a dilute electrolyte. If the pore size is too small or too large, it is not economically workable for the application of EOP. Equation 8 describes the velocity of the pore solution.

$$V_e = \frac{\varepsilon \xi E}{4 \pi \nu l} \tag{8}$$

16

Where:

V_e = flow velocity of solution (meters per second [m/s])

ε = dielectric constant of water (Farads per meter)

ξ = zeta potential (the difference of potential between the plates of a hypothetical capacitor used to model the diffuse layers in the capillary structure

E = potential applied across material (V)

v = viscosity of liquid (centipoise)

l = distance between electrodes (meters)

Based on this equation, observations are made regarding how to maximize the effectiveness of electro-osmosis [16]:

1. Maximizing the zeta potential through use of a porous material

2. Reducing the contamination of the ground water

3. Maintaining a saturated material

4. Limiting the hydrostatic pressure force

5. Minimizing the spacing between electrodes

6. Using nonpolarizing electrodes or a pulsed reversing system (EOP) in order to reduce the resistance in the vicinity of the electrodes

However, not all of these factors can be controlled with regard to existing structures in the field. Equation 9 expresses the same velocity in terms of current density.

$$V_e = \frac{\varepsilon \xi j}{4 \pi v \sigma} \tag{9}$$

Where:

V_e = flow velocity of solution (m/s)

ε = dielectric constant of water (Farads per meter)

ξ = zeta potential (V)

v = viscosity of liquid (centipoises)

j = current density (amperes per square meter)

σ = electrical conductivity of material (Siemens per meter)

In the electrolyte, the positive ions tend to be solvated, and the negative ions tend to be unsolvated [17-19]. Solvation is defined as the process of attraction and association of molecules of a solvent with molecules or ions of a solute, so as ions

dissolve in a solvent, they will spread out and are surrounded by solvent molecules. Thus, as the positive ions move through the pores, the water molecules will move with them and are dependent on the concentration of ions, type of material, and magnitude of the applied current [17-19]. The negative charge on the pore walls of the concrete sets up a capillary with an electrical double layer of cations dissolved in the pore fluid (figure 16). The application of a direct current (DC) electric field across the capillary causes the positive ions and the solution to move from the anode to the cathode as shown in figure 17a. The current must be applied to minimize alteration of the pore solution. Figure 17b is a sketch depicting EOP action in a pore.
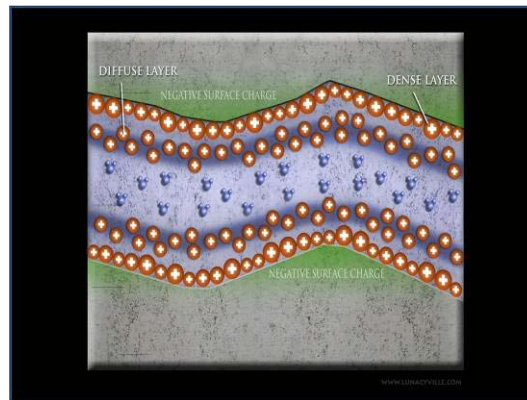

Figure 16. Illustration of concrete pore structures showing the electrical double layer of cations [1].
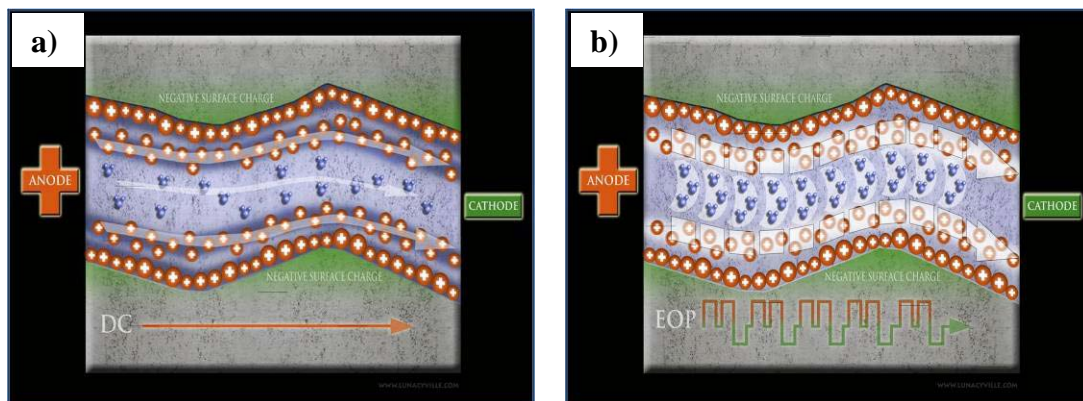

Figure 17. Illustration of concrete pore structures showing the application of DC voltage to move the cations and water (a) and the effect of EOP action in the pore (b) [1, 2].

However, new applications for this technology are still being developed. The electrical pulse causes cations (e.g., Ca++) and the associated water molecules they are dissolved in to move from the anode, installed on the dry side, towards the cathode, installed on the wet side as shown in figure 18. This will create a

type of barrier and prevent water molecules from entering the concrete structure as illustrated in figure 19. In the case of thick concrete, cathodes can be placed deep in the concrete section, such that the current and electric field pushes against the direction of flow induced by the hydraulic gradient, preventing water penetration through buried concrete structures. In order to overcome the force exerted on the water molecules by the hydraulic gradient a certain current density is required, creating sufficient electric field strength in the concrete.
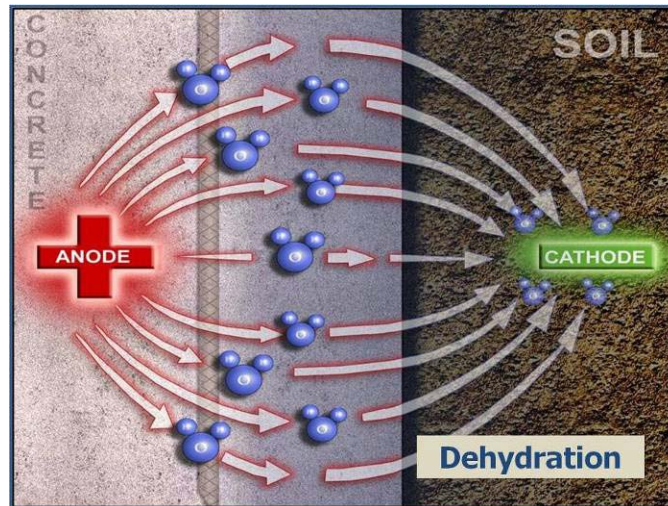

Figure 18. Illustration of cations and water molecules moving from anode to cathode on a macro scale with the application of EOP to dehydrate concrete [1].
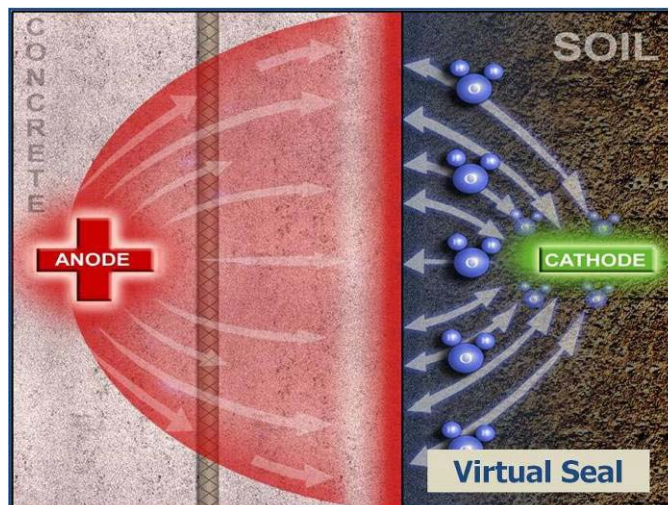

Figure 19. Illustration of the effects of the application of EOP to create a virtual seal or barrier to prevent water from entering the concrete on a macro scale [1].

A commercial system was developed, based on a Polish patent, to apply EOP technology using the application of a pulsating direct electric field, combined with an off period, to reverse the flow of water seepage. The pulse sequence consists of a pulse of positive voltage (as seen from the dry side of the concrete wall), a period of rest when no voltage is applied, another positive pulse, and then a pulse of negative voltage. The voltage pulse prevents the alteration of the chemical composition of the pore solution due to the application of the current [20]. Retaining some moisture in the interior helps to maintain the chemistry of the pore solution [20].

A balance of the anode/cathode current density must be maintained to control the water seepage without generating gas and acid at the anodes [20]. The generation of acid causes degradation of the anode material, as well as the cement paste adjacent to the anode [20]. It is well known that the pH can change dramatically in the vicinity of the electrodes during electro-osmosis [21]. The typical anodic reaction of oxidation of hydroxyl ions, shown in equation 10, begins with producing water molecules, oxygen, and electrons.

$$4OH^- \rightarrow 2H_2O + O_2 + 4e^- \qquad \textbf{(10)}$$

These are transferred to the cathode via the system metallic path. The process uses up hydroxyl ions at the anode and, therefore, the concentration of hydrogen ions increases, which often drops the pH of the concrete around the anode to values lower than 5 [20]. Figure 20 shows a representative plot of the pH evolution at the anode and cathode for concrete and montmorillonite cell [22].
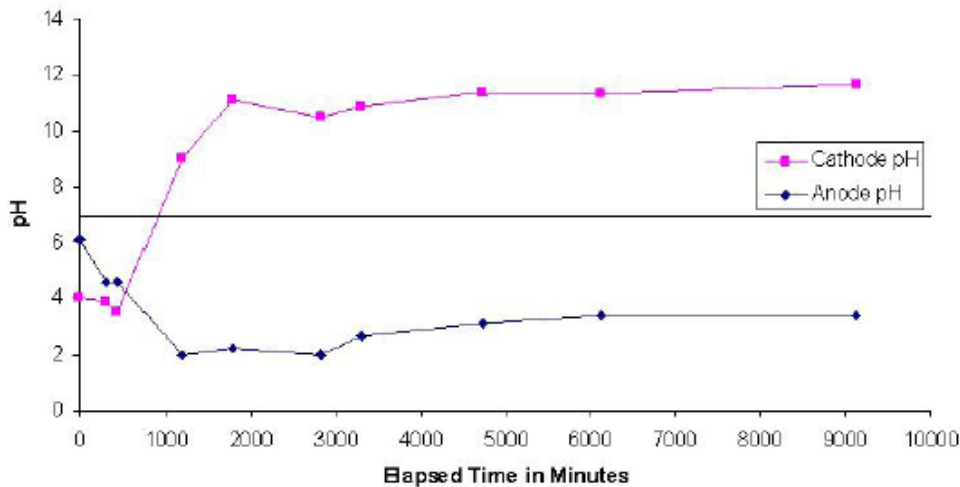

Figure 20. A representative plot of the measured pH at anode and cathode wells for concrete and sodium montmorillonite cell [22].

The amount of moisture in the concrete is controlled by the negative voltage pulse to prevent overdrying of the concrete matrix and subsequent degradation [20]. A

pulse sequence consists of a pulse of positive voltage (as seen from the dry side of the concrete wall) for 0.5 second, a period of rest when no voltage is applied, another positive pulse, typically 6 seconds in duration, and then a pulse of negative voltage lasting 0.5 second [20]. The amplitude of the signal is typically on the order of 20 to 40 volts direct current (V_{DC}) [20]. Figure 21 shows a typical EOP pulse wave form sequence.
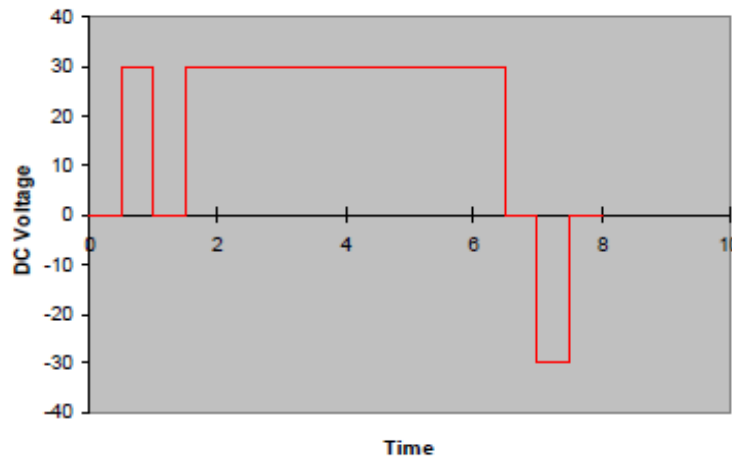

Figure 21. Typical EOP wave form showing the positive pulses, negative pulse, and rest period [2].

Cost/Benefit Analysis

As stated earlier, damage due to water seepage through concrete can cause extensive and expensive damage. Necessary repair work can include excavation, trenching, grouting, coating, major concrete repair for rebar corrosion issues, etc. An analysis can be made to determine the cost/benefit of installing an EOP system. This is a fairly simple method for approximating any cost savings and does not include the cost of any compounded degradation issues. In addition, it may not account for all costs due to disruption and lost productivity. The percent savings calculated using equation 11 is based on the capital costs and, in simple terms, is the comparison between the cost of repair and installing an EOP system [20, 23].

$$\% \text{ first cost saved} = 100 \times \left(1 - \frac{\text{EOP per linear foot}}{\text{Repair per linear foot}} \right) \tag{11}$$

Another important calculation would be that of payback or the time it takes to recoup the investment based on the overall reduction in cost for repair and maintenance. There are two different methods used for determining this: Payback Upon Price Comparison (P_{PC}) and Payback Over Time (P_{OT}) [20, 23]. The price comparison method shown in equation 12 is used to determine the length of time to save the investment for the EOP installation compared to the cost of repair [20, 23]. The over time method shown in equation 13 is more

involved and is a comparison between the EOP installation cost and the sum of all annual costs avoided over a specified length of time due to the EOP system [20, 23].

$$P_{PC} = \cfrac{1}{\cfrac{\text{Repair per linear foot - EOP per linear foot}}{\text{EOP per linear foot}}} \qquad (12)$$

$$P_{OT} = \cfrac{\text{Total Installation Cost}}{\text{Sum of Annual Cost Avoidances}} \qquad (13)$$

It is important to understand that these are only approximations. However, they can be used to determine the effectiveness of the installation of EOP compared to the required continual maintenance.

EOP Components at Trinity

Strip Type Anodes and Cathodes

Mixed metal oxide coated titanium mesh material is used for the strip anode and cathode material. The mesh is spot or resistance welded to a titanium bar, and the bar is welded to a titanium rod. The lead wire is attached to the titanium rod using a crimp type connection and is encased in shrink wrap tubing. Figure 22 shows a schematic of an electrode.
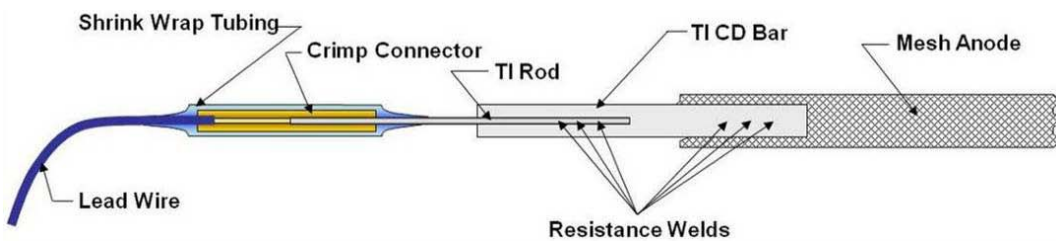

Figure 22. Schematic of the mixed metal oxide coated titanium mesh electrode, which can be used for both an anode and cathode [1].

For the Trinity installation, strip anodes were approximately 7 feet long and ½ inch wide. A red insulated cable was used for the anodes. Figure 23 shows anode materials installed on this project. Strip cathodes were approximately 12 inches long and ½ inch wide. A green insulated cable was used for the cathodes. Figure 24 shows cathode materials installed on this project.
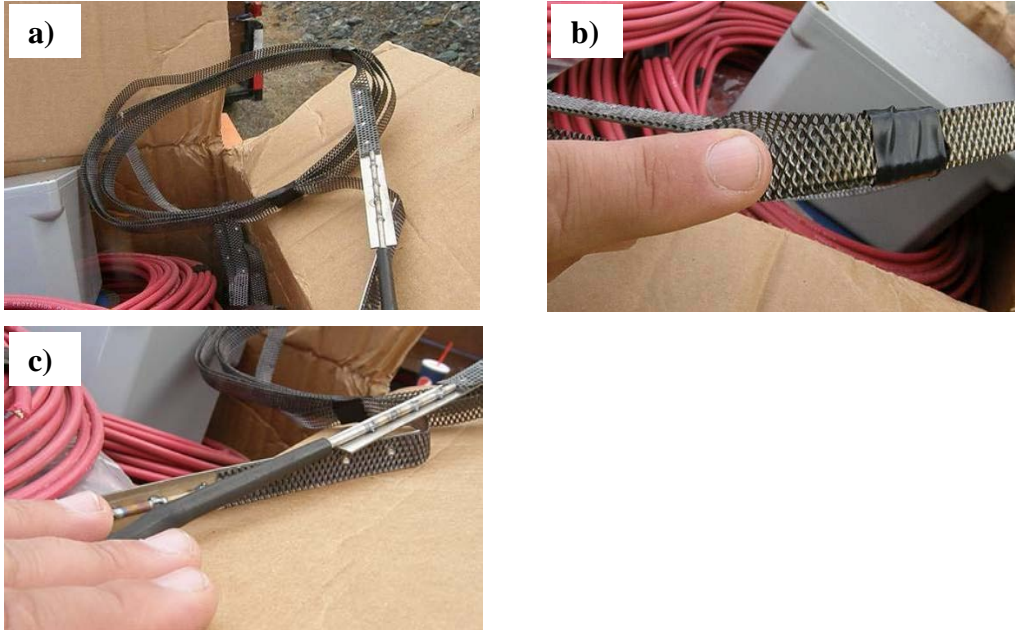
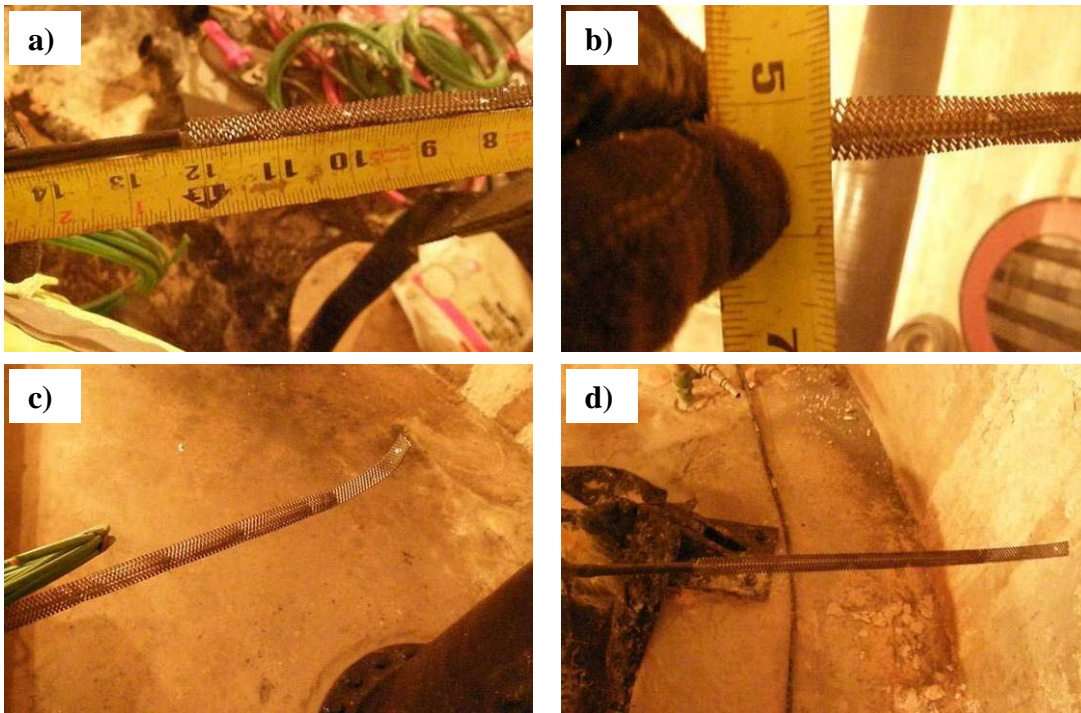**Figure 23. Mixed metal oxide coated titanium mesh strip type anodes installed in the concrete wall.**

Figure 24. Mixed metal oxide coated titanium mesh strip type cathodes installed in the concrete wall.

Probe Type Anodes

Probe anodes were approximately 6 to 7 inches long and a little under ½ inch in diameter. The material was a mixed metal oxide coated titanium mesh formed into a tube shape. The probe electrodes had a screw type connection on one end to attach the lead cable. Figure 25 shows a probe anode installed on this project.
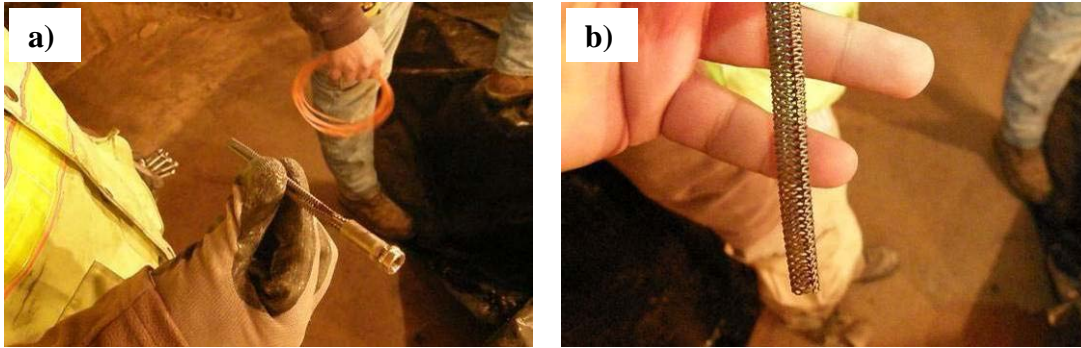
Figure 25. Mixed metal oxide coated titanium mesh probe type anodes installed in the concrete wall.

System Controller

The system controller is powered by a 120 V_{AC} circuit. Data is collected continuously by the controller and is stored on a secure digital memory (SD) card, which can be removed to easily download data for analysis. The controller contains a rectifying unit for changing the AC to DC, a surge protector, and the necessary electronics to set the output potential and pulse cycles. Figure 26 shows the unit used for the Trinity Dam system.

Figure 26. DC voltage controlled pulse unit installed at Trinity Dam for the EOP system.

Chapter III

Installation of EOP at Trinity

Calcite Removal

The calcite deposits on the bonnet chamber wall opposite the hatched doorway were removed using a chipping hammer and a grinder (figures 27a and 27b). The area cleared off was approximately 14 feet wide and 6 ½ feet high starting from the floor. Removal of calcite required roughly 1 day, due to the sheer volume, as shown in figure 27c. The calcite came off the wall in chunks. The calcite deposits on the wall were an average of 0.5 to 1 inch in thickness as shown in figure 27d.

Figure 27. Removal of calcite from the concrete wall in the bonnet chamber using a chipping hammer (a) and grinder (b). The volume of calcite removed is shown in (c). Deposits on the wall were an average of 0.5 to 1 inch thick (d).

Anodes

Two types of anodes were used during this phase to see which would be most effective but we were not able to determine any difference.

Strip Anodes

Four strip anodes were installed in the test section. The anode material was installed in the wall at the floor joint and 6 feet above the floor. Two strips were installed at each location to cover the entire 14 feet.

A groove approximately 1 inch wide by 1 inch deep was cut in the concrete 6 feet above and parallel to the floor using a circular saw as shown in figures 28a-28d. A vacuum system was hooked up to the saw to minimize the concrete dust created during the saw cut. A second groove was cut approximately 6 inches above the anode groove for a water drip strip. The weather strip shown in figures 29a and 29b was installed to prevent water from the wall above from flowing over the test area, which might lead to erroneous readings. The anodes with lead wires attached (see figure 23) were inserted in the groove, and the groove was filled with a Portland cement grout (BASF Masterflow 928). Figures 30a-30c shows the installation of the upper strip anodes. The grout was smoothed flush with the wall with an anode cable at each end of the groove (figure 30d).
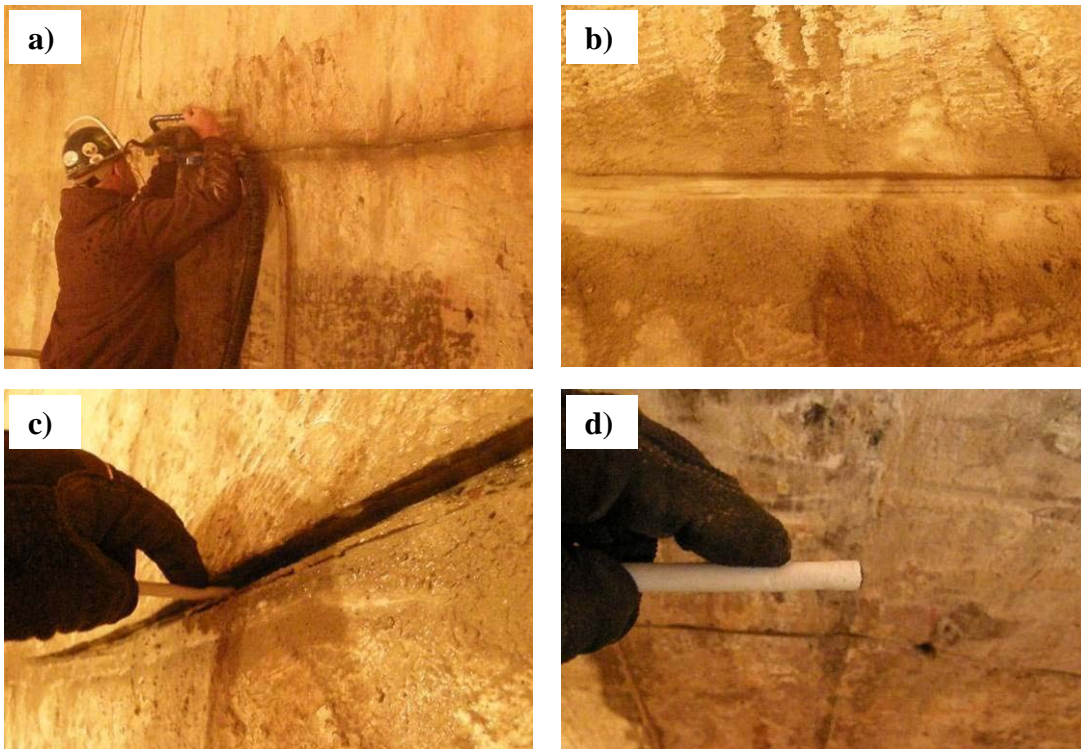

Figure 28. a) and b) show saw cutting of groove for strip anode installation. The finished groove, approximately 1 inch in depth, is shown in c), d), and e).

28

Figure 29. Installation of weather strip to act as a drip tray for water dripping down from above.
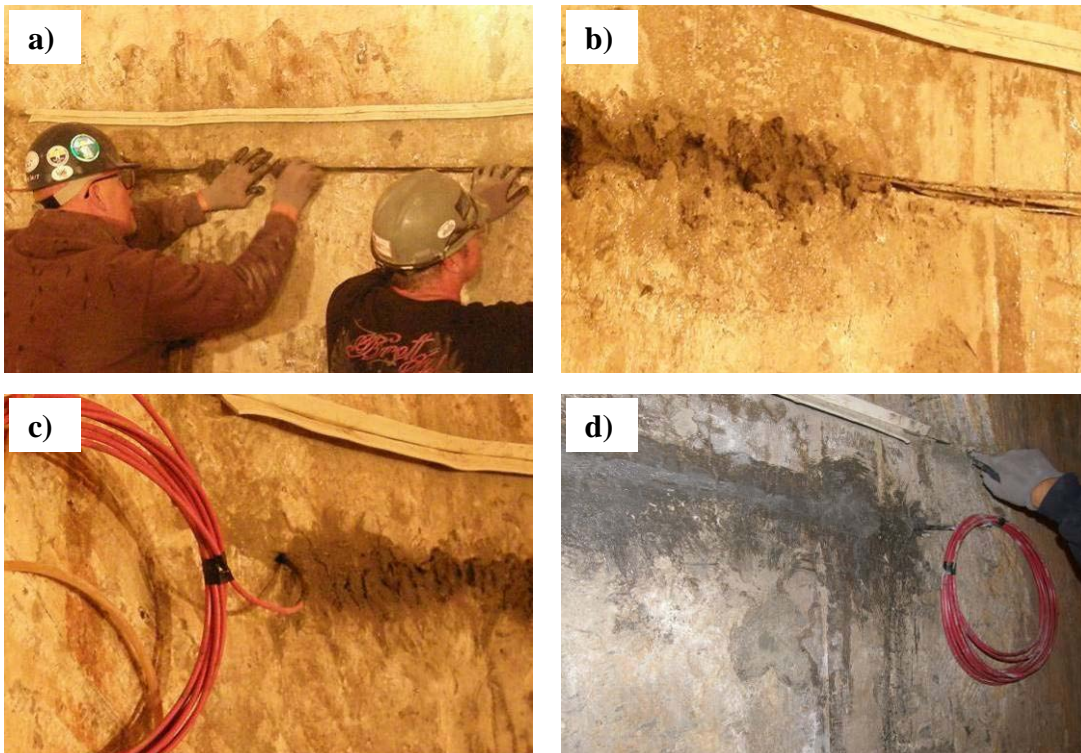

Figure 30. Installation of upper strip anode and hand packing of Portland cement grout into the groove shown in photos a), b) and c). Photo d) shows finished installation of upper anode strips and cable.

A groove about 1 inch deep was chipped out along the floor using a chipping hammer to accommodate a strip anode (figures 31a and 31b). The anodes with lead wires attached (figure 23) were inserted in the groove along the floor. Then, the groove was filled with a Portland cement grout (BASF Masterflow 928). Figures 32a-32c show the installation of the lower strip anodes. The grout was smoothed flush with the wall with an anode cable at each end of the groove (figure 32d).

Figure 31. Groove for floor joint chipped out using chipping hammer to create a groove approximately 1 inch in depth.
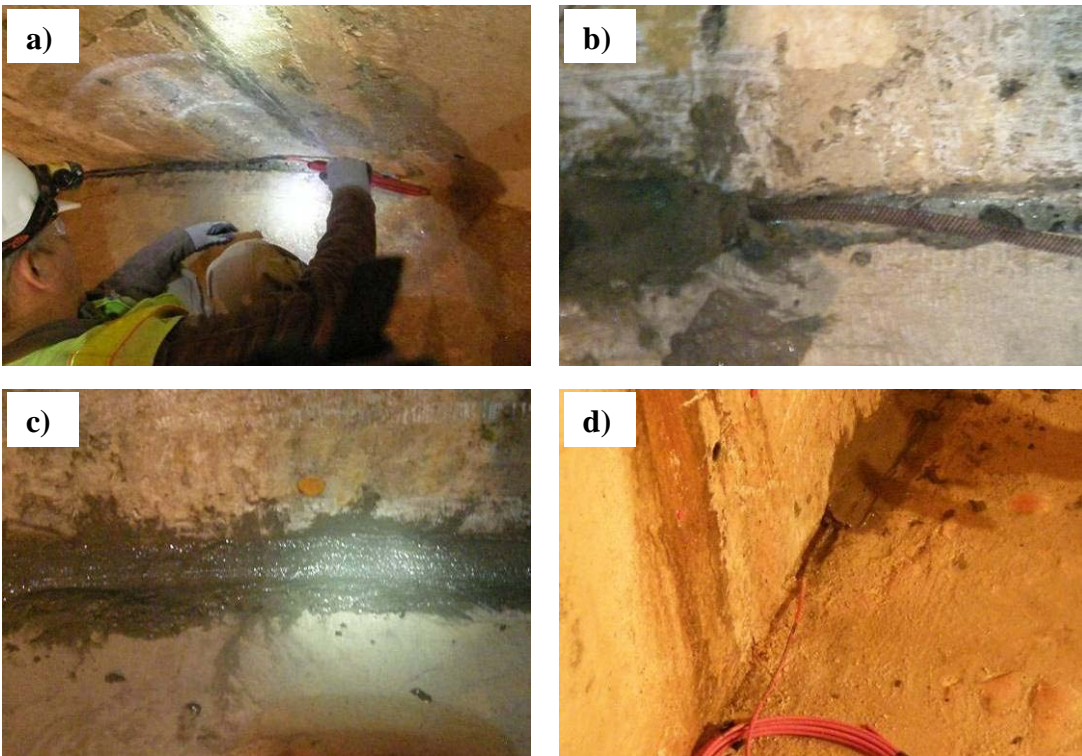

Figure 32. Strip anodes were installed in groove and then packed with a Portland cement grout.

Probe Type Anodes

Seven holes (⅞ inch in diameter) were drilled approximately 3 feet above the floor and approximately 2 feet apart (figure 5 and figure 33a). The holes were drilled to a depth of approximately 6 to 7 inches to accommodate the probe anodes. A groove was cut into the wall joining all the holes to embed the anode header cable as shown in figure 33b. The probes were inserted into the holes and connected to a single header cable shown in figures 34a-34c. The probe holes were then filled with grout, and the header cable was placed in the groove and filled with grout as shown in figures 34d-34f. The probe anode header cable was terminated in a junction box, connected to the other anode cables, and then connected to the main anode header cable, which connects to the system controller.
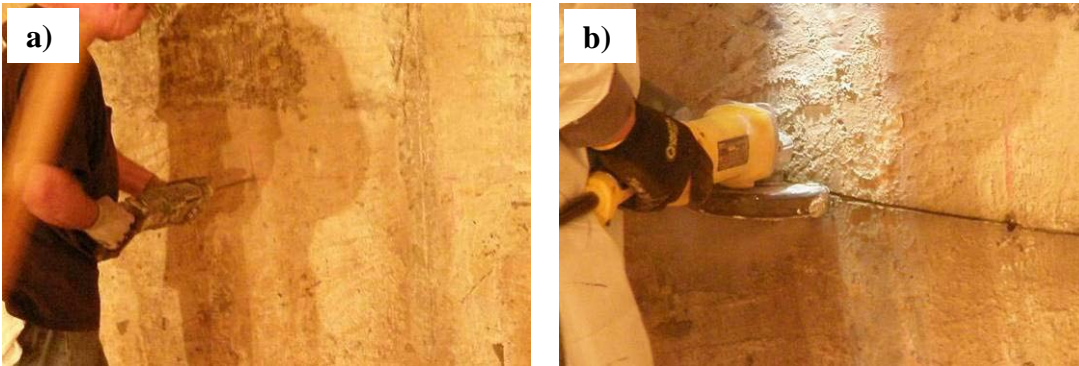

Figure 33. Holes were drilled for probe anodes as shown in a) and a groove was cut for embedding the cable as shown in b).
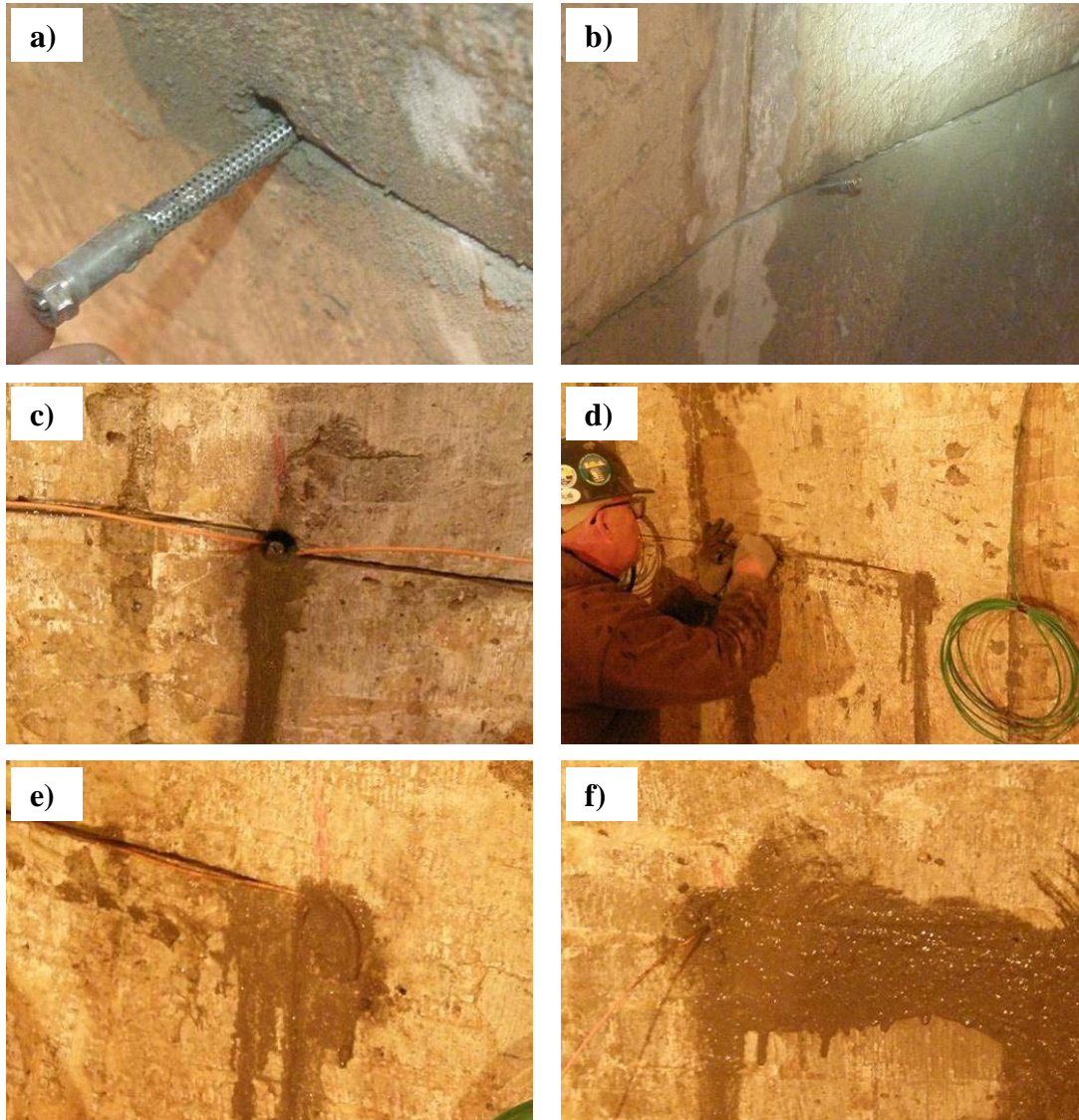
Figure 34. Probe anodes were inserted into the hole as shown in a) and b). The anodes were connected to a single header cable, which was placed in the saw cut groove as shown in c), d), and e). Portland cement grout was poured in the holes around the anodes, and the anodes and cable were grouted in as shown in e) and (f.

Cathodes

Eight holes ($\frac{7}{8}$ inch in diameter) were drilled to a depth of approximately 12 inches and at a slight downward angle for the cathode strips. Four holes were drilled approximately 1 foot above the floor, and four holes were drilled approximately 4 feet above the floor as shown in figure 5 and figures 35a and 35b. The cathode strips were cut to fit based on the actual depth of the hole. Then, the holes were filled with a Portland cement grout. Figures 36a - 36c show the installation of the cathodes and grouting.

The cathode holes were placed at an equal spacing along the test section, approximately 3 feet 10 inches apart as shown in figure 5, and the top row was slightly offset from the bottom row. Figure 5 and figure 37 show the locations of the cathodes.
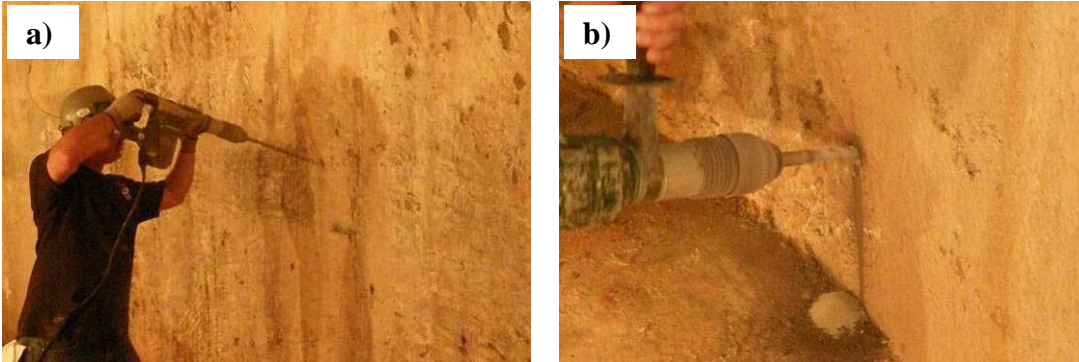

Figure 35. Drilling holes for cathode installation. Note the slight downward angle.
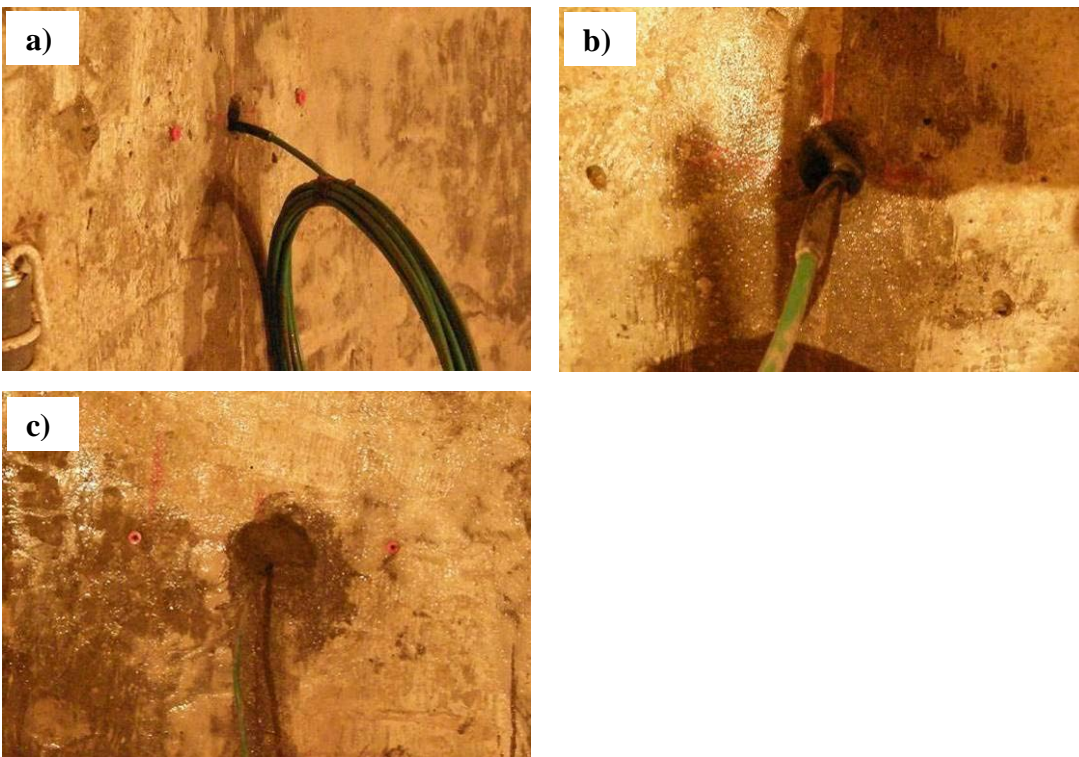

Figure 36. Installation and grouting of cathodes.

Technical Memorandum No. MERL-2012-10
Electro-Osmotic Pulse Leak Repair Method: Evaluation in Trinity Dam Bonnet Chamber

Figure 37. Locations of cathodes (green cables) in relation to each other and to anodes (red cables).

Junction Boxes

Junction boxes were installed at each cathode location (figures 38a and 38b). The cathode cables were then run through the junction boxes (figures 39a and 39b). The anode cables were placed and grouted into grooves cut into the wall and into the cathodes' junction boxes, and then they were run in the same conduit as the cathode cables shown in figures 40a and 40b.

The rebar was located, and a hole was drilled in order to expose one of the bars. A tapped connection was then made to the rebar as shown on the left side of figure 39b. This connection allows the system to supply the rebar with a small amount of protective current and prevents any damage to the rebar due to operation of the system.

All the cables were terminated in a main junction box. Figure 41 shows cables being connected to header cables in the main junction box. The cathode cables were connected to a main cathode header cable, all the anode cables were connected to a main anode header cable, and the main header cables and a cable connected to the rebar were run through conduit to the system controller. Figure 42 shows the complete installation of all electrodes and junction boxes.
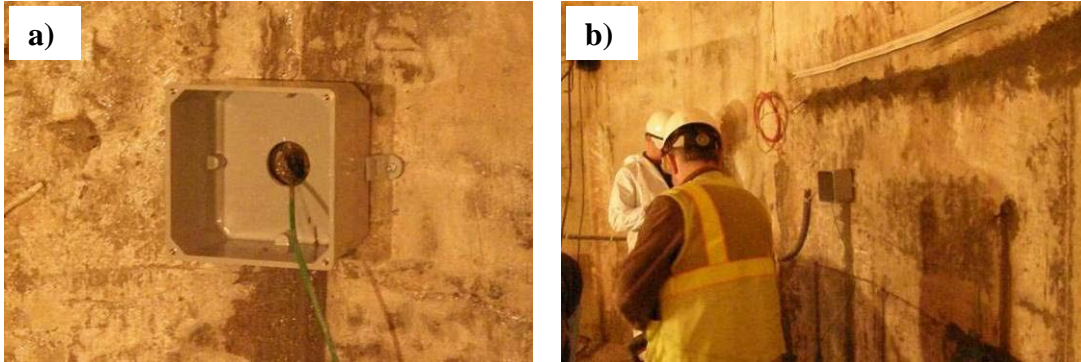
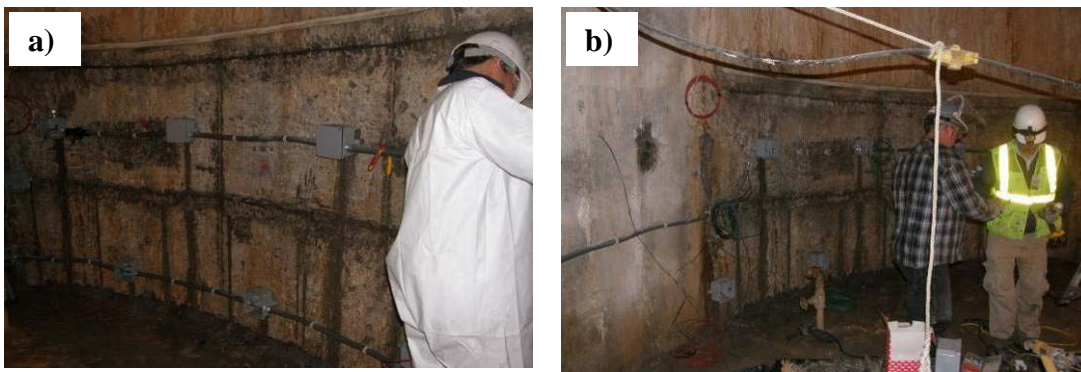**Figure 38. Installation of junction boxes and wiring of system.**

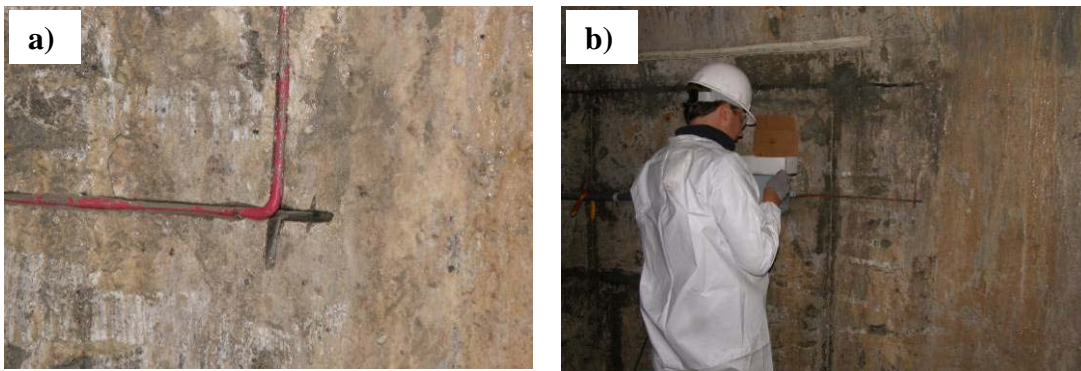**Figure 39. Cables were run through conduit to main junction box.**

Figure 40. Anode cables were embedded into the wall to the cathode junction box, and cable was run through the same conduit as the cathode cables.

Figure 41. All cables were terminated in a main junction box. The cathode cables were connected to a main cathode header cable, all the anode cables were connected to a main anode header cable, and the main header cables and a cable connected to the rebar were run through conduit to the system controller.

Figure 42. Completed installation with junction boxes and conduit.

Permanent systems only include one junction box and conduit to a control unit, depending on the size of the structure. The anode cables are embedded in the concrete wall, and the cathode cables would either be embedded in the concrete wall or buried, depending on the location of the cathodes and control unit.

System Control Unit and Power

The control unit was mounted on the wall just outside of the hatch for the bonnet chamber to prevent collection of water and calcite on the unit as shown in figure 43a. Figure 43b shows the internal components of the unit to include the location of the SD card used for storage of the collected data. The card is located on the side behind the front panel. The conduit containing the anode header cable, cathode header cable, and the cable for the rebar connection was installed between the EOP test section along the wall and through the open hatch to the control unit. The control unit was wired into a 120 V_{AC} power source, using a series of extension cords, to an outlet at the top of the shaft approximately 420 feet away. Figure 44 shows the conduit containing the cables and the yellow electrical cord for the power.
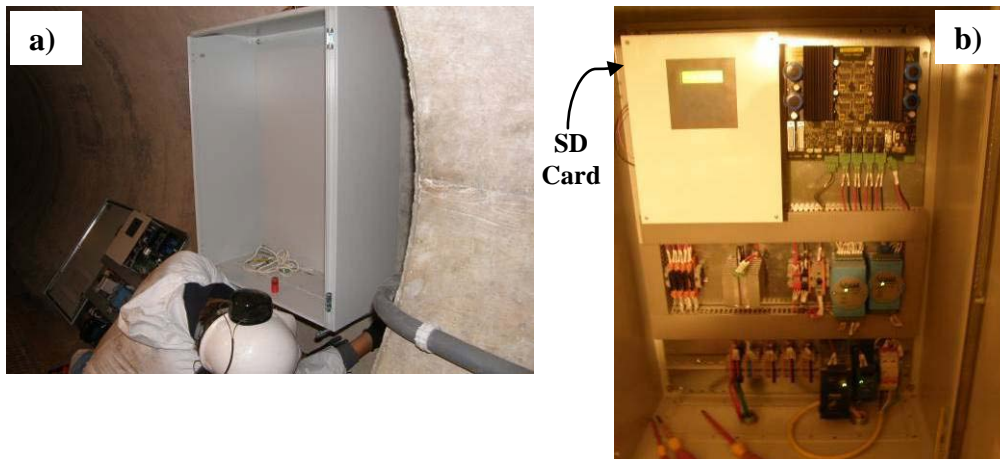

Figure 43. The cabinet was installed on the wall outside the chamber as shown in a). Photo b) shows the internal components of the unit. The arrow points to the location of the SD card used for data storage.

Figure 44. The conduit containing the anode header cable, cathode header cable, and rebar cable. The unit is powered by the yellow extension cord wrapped around the conduit.

The system was activated and programmed for operation on September 29, 2011, at 11:37 a.m. as shown in figures 45a and 45b. The unit was programmed to hold a potential of 24 V_{DC} with a current applied to the rebar of approximately 1-2 milliamperes (mA).
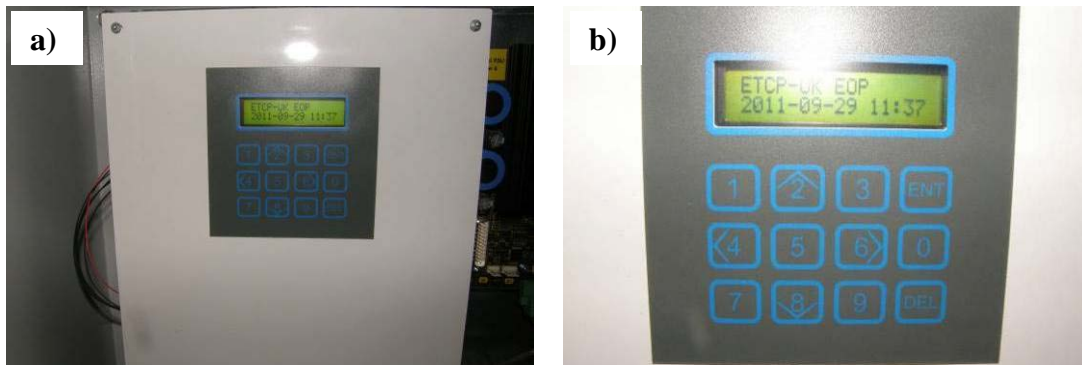

Figure 45. The photos show the operational unit, noting the date (2011-09-29) the unit was energized.

Chapter IV

Test Data

As-Left Condition

The wall of the chamber where the test section was located showed a saturated or wet concrete, both to sight and touch, as shown in figures 46a and 46b. These photos were taken to document wall moisture conditions to help determine if the system was operating using visible wall moisture conditions.
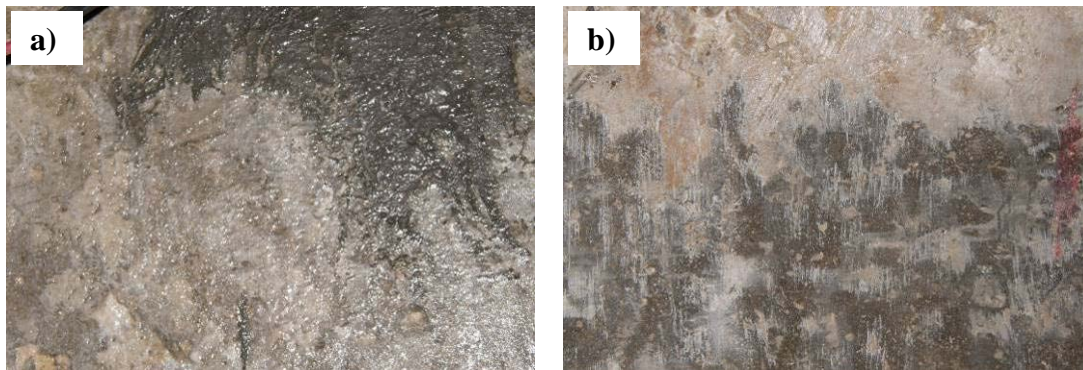

Figure 46. Condition of wall at installation location after installation prior to energizing of the system. Note the wall was damp to sight and touch.

Initial Two Weeks of Operation

On October 12, 2011, after about 2 weeks of operation, the system was evaluated and data collected from the SD card. Figures 47a- 47d all show dry areas of concrete after 2 weeks of operation. Figure 47b still shows an area where the concrete appears damp. The humidity in the chamber is nearly 100 percent due to high levels of water and moisture in the chamber. The weatherstrip installed to act as a drip tray was full of water and had calcite in it, as shown in figure 47c. The tray was not draining as designed, causing water to drip down onto the wall below in some areas as shown in figure 47d. The water primarily was dripping down onto one of the center junction boxes.

The unit collects and saves data to the SD card in an Excel spreadsheet format every 4 hours. Each file contains all the data for a single month. Table 2 shows an example of the data collected in the month of October. The collected data is then analyzed using Ohm's law $E = IR$, where E is the potential (V), I is the current (A), and the R is resistance (ohms). Over time, at a constant applied potential, the current will decrease and the resistance will increase as the moisture level in the concrete decreases in the wall. Figure 48 shows that over the initial first 2 weeks of operation, the measured total current decreased and the calculated

resistance increased. The data trend shown in figure 48 indicates that the system is operating as designed. Observations of wall moisture also indicated that the wall was drying as shown in figures 47a-47d.
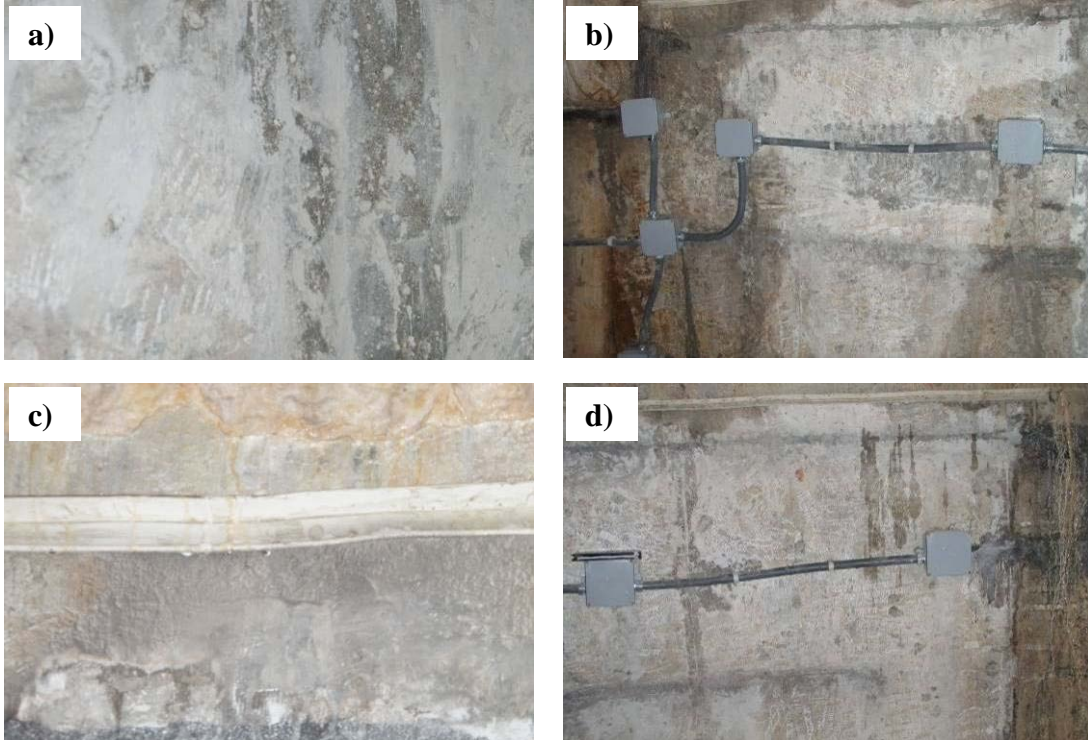

Figure 47. Concrete wall at location of installation after 2 weeks of operation. The wall was dry to sight and touch over most of the test section as shown in a) and b). Damp areas and drips, as shown in b) and c), resulted because the drip tray was filled up with calcium carbonate saturated water and unable to drain properly as shown in d).

Table 2. Example data collected for the beginning of October

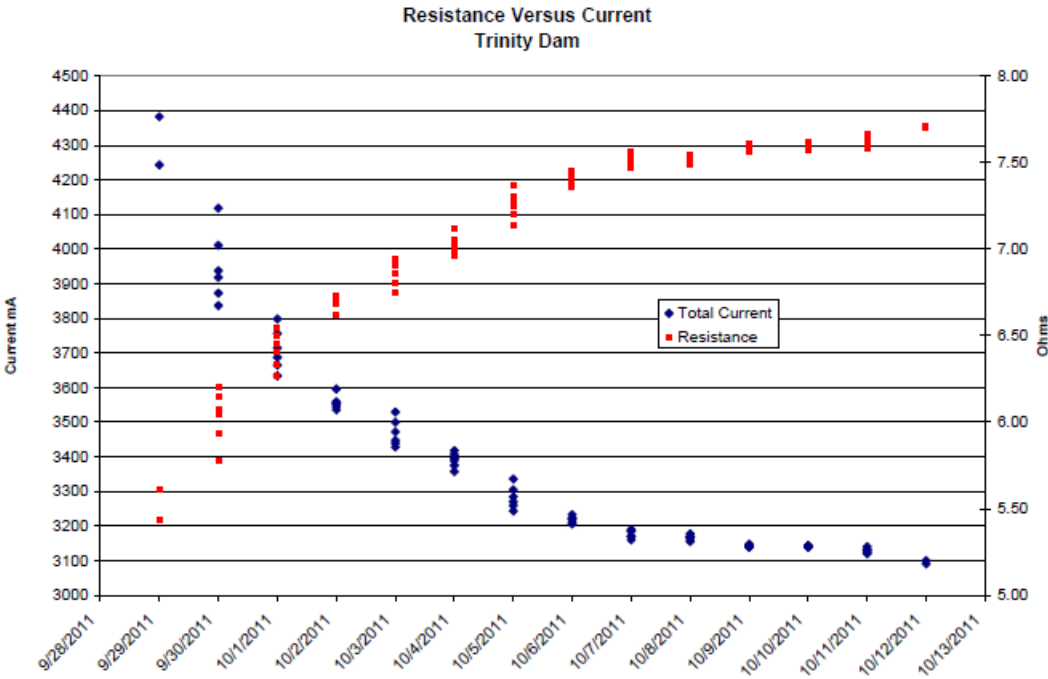| Date	Time	Voltage (V)	Total Current (mA)
10/1/2011	0:00	23.8	3,798
10/1/2011	4:00	23.8	3,756
10/1/2011	8:00	23.8	3,714
10/1/2011	12:00	23.8	3,687
10/1/2011	16:00	23.8	3,665
10/1/2011	20:00	23.9	3,634
10/2/2011	0:00	23.8	3,596
10/2/2011	4:00	23.8	3,559
10/2/2011	8:00	23.8	3,546
10/2/2011	12:00	23.8	3,554
10/2/2011	16:00	23.8	3,555
10/2/2011	20:00	23.9	3,536
10/3/2011	0:00	23.8	3,529

Figure 48. Data from the first 2 weeks of system operation showing the current and resistance over time. The data shows that the moisture content in the concrete is decreasing over time.

Five Weeks of Operation

Data was collected after 5 weeks of operation to determine operation and the current and resistance trend for the system. Figure 49 shows the analyzed data for total current output and resistance. The total current continues to decrease, and

the resistance continues to increase. This indicates that the system is still operating as planned and the moisture content of the concrete continues to decrease. The resistance calculated after 5 weeks of operation is nearly double its original value.
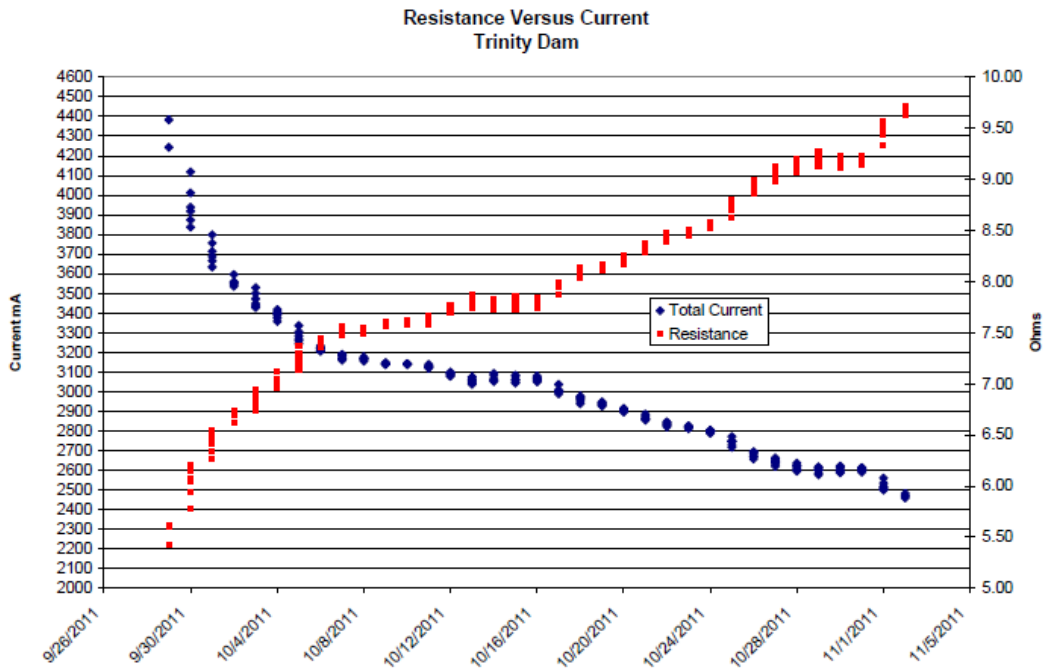

Figure 49. Data from the first 5 weeks of system operation showing the current and resistance over time. The data shows that the moisture content in the concrete is decreasing.

Eleven Weeks of Operation

Data was collected after 11 weeks of operation to determine operation and the current and resistance trend for the system. Figure 50 shows the analyzed data for total current output and resistance. The total current continues to decrease, and the resistance continues to increase. This indicates that the system is still operating as planned and the moisture content of the concrete continues to decrease. The resistance calculated after 11 weeks of operation is almost 2.5 times larger than its original value.
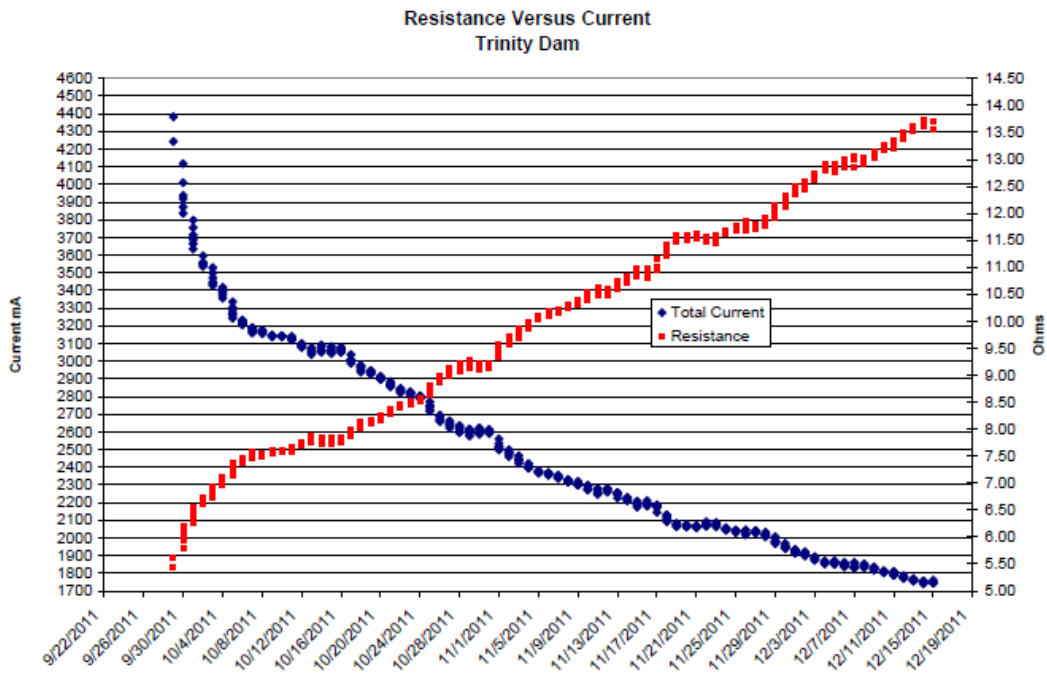
Figure 50. Data from the first 11 weeks of system operation showing the current and resistance over time. The data shows that the moisture content in the concrete is decreasing.

Fifteen Weeks of Operation

Data was collected after 15 weeks of operation to determine operation and the current and resistance trend for the system. Figure 51 shows the analyzed data for total current output and resistance. The total current continues to decrease, and the resistance continues to increase. This indicates that the system is still operating as planned and the moisture content of the concrete continues to decrease. The resistance calculated after 11 weeks of operation is almost 3 times larger than it was originally. Visual observations shown in figures 52a-52c indicate that the test section wall is dry, except where water is dripping down from the overflowing drip tray. The drying of the surface of the wall can be observed when comparing a location after 2 weeks (figure 47b) to the same location after 15 weeks (figure 52a). Note the buildup of calcite where water is dripping down at the end of the drip tray shown in figure 52c compared to the photo taken of the same area after 2 weeks (figure 47d). The drip tray is overflowing, and water is dripping down onto the wall and junction boxes in some locations. The streaks from the overflowing water on the drip tray, shown in figure 53, indicate that the water is rich in calcium.
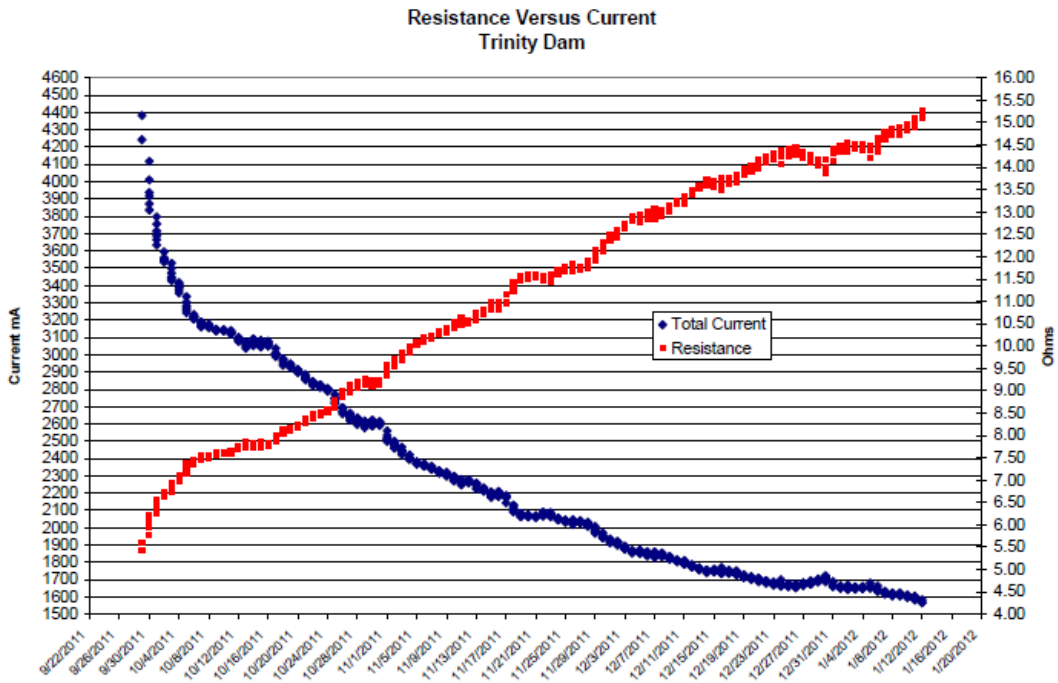
Figure 51. Data from the first 15 weeks of system operation showing the current and resistance over time. The data shows that the moisture content in the concrete is decreasing.
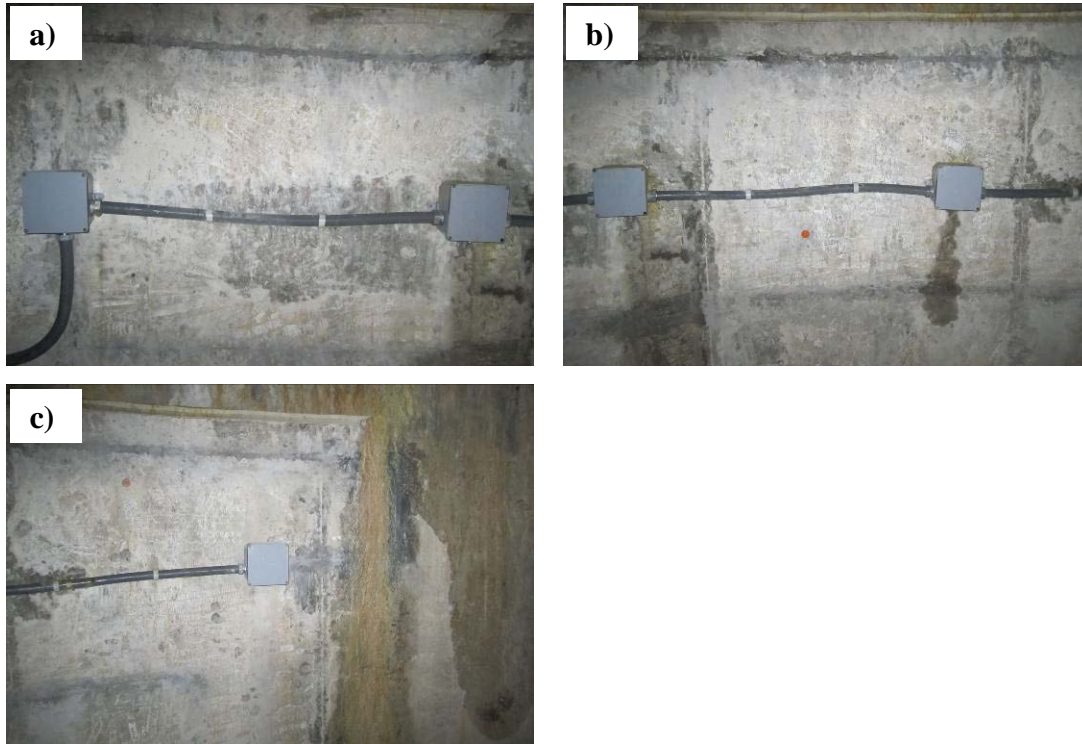
Figure 52. Concrete wall at location of installation after 15 weeks of operation. The wall was dry to sight and touch over most of the test section as shown in a), b), and c). The observed damp areas and drips resulted because the drip tray was filled up with water and unable to drain properly. Note the new buildup of calcite on the wall at the end of the drip tray in c).

Figure 53. Visible water overflowing the drip tray, allowing water to fall onto the wall and junction boxes below. Note the color of the streaks of water, indicating that the water is rich in calcium carbonate.

Determination of Decreasing Concrete Corrosivity

The resistance calculated from the power supply output using Ohm's law (resistance equals voltage divided by current), shown in figure 49, was compared

to the resistance calculated using equation 14 at various resistivities. The comparison is shown in figure 54 and indicates that the resistance calculated from the power supply follows a similar trend to the linear calculation for resistance (R_{ra}). The trend indicates that the resistivity is increasing over the operation period, as shown in figure 55, after 11 weeks of operation. Resistivity is often used to help determine the possible corrosivity of the environment. Results indicate that the concrete has become a less corrosive environment for the rebar.

$$R_{ra} = \left(\frac{0.00521\rho}{NL}\right)\left(\ln\left(\frac{4L^2 + 4L\sqrt{S^2 + L^2}}{dS}\right) + \frac{S}{L} - \frac{\sqrt{S^2 + L^2}}{L} - 1\right) \qquad \textbf{(14)}$$

Where:
N = number of anodes
L = length of anode, feet
D = diameter of anode, feet
S = twice the depth of the anode, feet
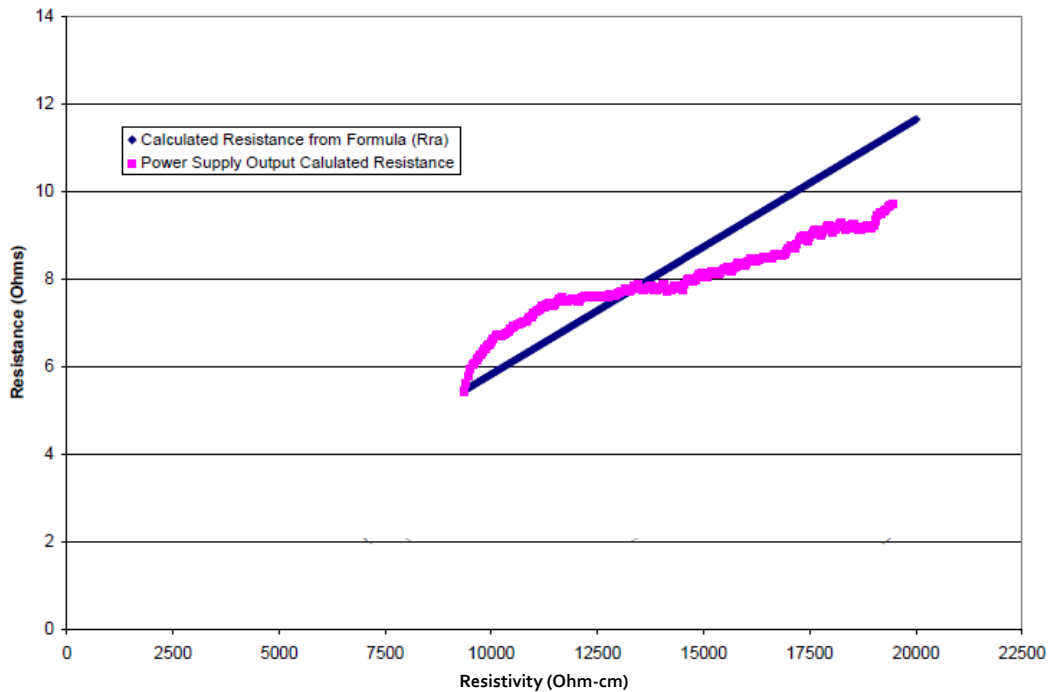P = material resistivity

Figure 54. Calculated resistance using equation 14 versus the resistance calculated using the actual power supply outputs.
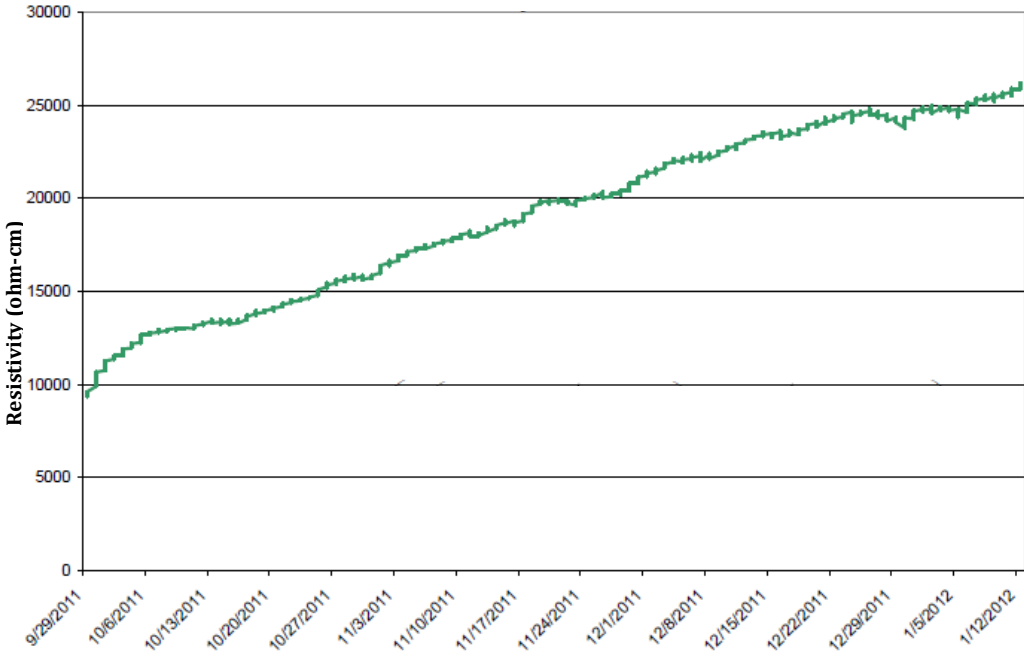
Figure 55. Calculated resistivity over the period of 15 weeks of operation.

Chapter V

Future Work

Phase Three

We recommend a phase three trial test location containing cracks and deeper calcite deposits. The proposed location for the next test section is the entire circumference of the bottom 10 feet of the shaft as shown figure 56. Cracks are desired in the next test section to show that after crack repair has been performed, the EOP system will work and improve long-term water tightness in the locations where cracks were grouted.
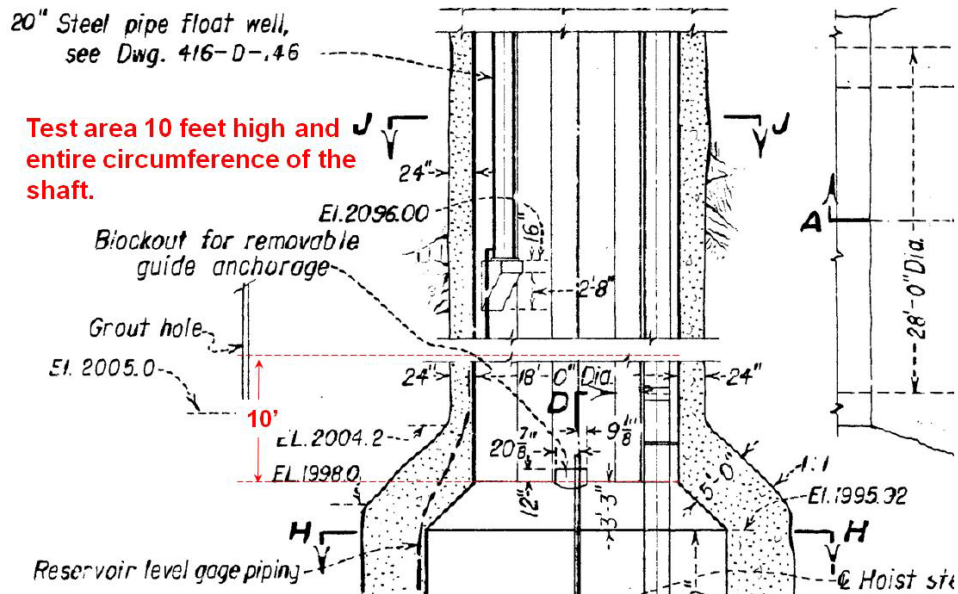

Figure 56. Proposed test section area for phase three of the EOP study.

Petrographic Analysis and Core Testing

Core samples should be taken from the lower chamber wall to analyze the concrete. Three 6-inch-diameter concrete samples should be collected and tested for composition and traditional core testing. The results will be used to mathematically evaluate the resistance against expected water content and, subsequently, estimate the humidity in the concrete. Figure 57 is an example graph showing the relationship for a different concrete composition and properties. The concrete testing will be performed by Materials Engineering Research Laboratory personnel.
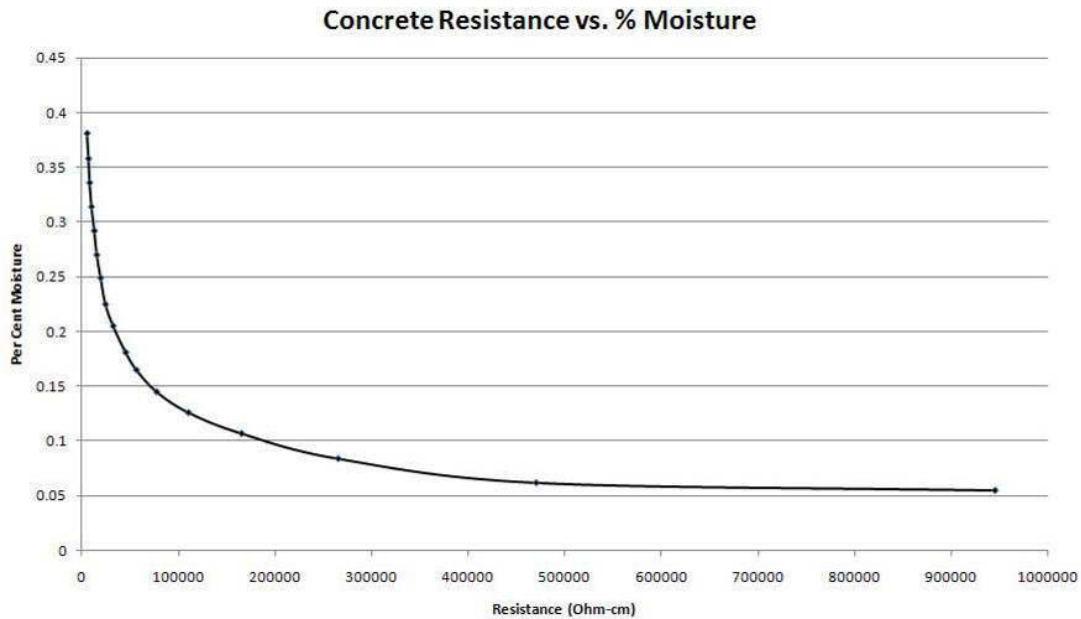
Figure 57. Example of relationship between concrete resistance and percent moisture in concrete [24].

Core testing to be performed should include the following:

- Water soluble chlorides – American Society for Testing of Materials (ASTM) C1218
- Acid soluble sulphate - ASTM C114
- Compressive strength - ASTM C42
- Air void analysis - ASTM C457
- Petrographic analysis - ASTM C856
- Specific Gravity

The petrographic analysis will include an identification of constituents, assessment of overall concrete quality, and investigation of potential causes of distress. In addition, features related to the original placement, such as approximate water/cement ratio, finish, consolidation, bleed, etc., are addressed where possible. Characterization of the occurrence and distribution of any secondary effects of water leaching, such as carbonation, aggregate reaction, sulfate attack, and their relationship to any visible distress, will be evaluated.

Cost Options

After discussions of the phase three test location, Electro Tech CP (contractor) supplied three cost options, which included a cost and extent of work for the given cost. Access issues and the need for scaffolding constitute a large portion of the cost. Approximately $65,000 of the cost is for erecting the necessary

scaffolding. These budget numbers do not allow for any cost by the U.S. Army Corps of Engineers, which would be a necessary addition. The U.S. Army Corps of Engineers' overhead is 54.8 percent, but this can be reduced to approximately 15 percent if we can use an Economy Act agreement.

Option A: Cost $225,000 ($398.23 per ft^2)
This includes work for a 10-foot-high area in the bottom of the shaft for the entire circumference for about 565 ft^2. This includes the scaffold cost and a budget number for crack injection of $20,000.

Option B: Cost $275,000 ($138.96 per ft^2)
Similar to Option A, but with an additional 25 feet in height, providing a total area of 565 ft^2 (Option A) plus 1,414 ft^2, totaling 1,979 ft^2. This includes the scaffold cost and crack injection.

Option C: Cost $102,000 ($680.00 per ft^2)
Similar to Option A, but with a reduced scope of only 15 linear feet around the circumference, similar to the current trial, and 10 feet in height (150 ft^2). This includes the scaffold cost and crack injection.

References

[1] Noyce, P., Personal communication, General EOP system figures, Electro Tech CP, LLC, Accord, New York, 2011.

[2] Marshall, O.S., S. Morefield, M. McInerney, and V.F. Hock, "Electro-Osmotic Pulse Technology for Corrosion Prevention and Control of Water Intrusion in Below Grade Concrete Structures," Tri-Service Corrosion Conference, Denver, Colorado, 2007.

[3] U.S. Army Corps of Engineers, "Electro-Osmotic Pulse (EOP) Technology - Product Sheet," Engineer Research and Development Center, Champaign, Illinois, 2005.

[4] Kosmatka, S.H., and M.L. Wilson, *Design and Control of Concrete Mixes, EB001, The Guide to Applications, Methods, and Materials,* 15th edition, Portland Cement Association, Skokie, Illinois, 2011, pp. 48-52, 165-176.

[5] Lea, F.M., *The Chemistry of Cement and Concrete,* 3rd edition, Chemical Publishing Company, Inc., New York, New York, 1971, pp. 177-249.

[6] Taylor, W.H., *Concrete Technology and Practice,* 2nd edition, Angus & Robertson Ltd., Sydney, Australia, 1967, pp. 249-257.

[7] Thomas, J., and H. Jennings, "The Science of Concrete," Northwestern University, Evanston, Illinois, 2008.

[8] Powers, T.C., "The Nonevaporable Water Content of Hardened Portland Cement Paste - Its Significance for Concrete Research and Its Method of Determination," Research Department Bulletin RX029, Portland Cement Association, Skokie, Illinois, 1949.

[9] Scherer, G.W., "Theory of Drying," *Journal of the American Ceramic Society*, Vol. 73, No. 1, 1990, pp. 3-14.

[10] McMillan, F.R., and I. Lyse, "Some Permeability Studies of Concrete," *Journal of the American Concrete Institute, Proceedings*, Vol. 26, 1929, pp. 101-142.

[11] Reuss, F.F., Memoires de la Societe Imperiale des Naturalistes de Moscou, Vol. 2, 1809, p. 327.

[12] Glasstone, S., *Textbook of Physical Chemistry*, 2nd edition, Van Nostrand Company, Inc., Princeton, New Jersey, 1946.

[13] Hamill, W.H., R.R. Williams, and C. MacKay, *Principles of Physical Chemistry,* 2nd edition, Prentice-Hall, Inc., Englewood Cliffs, New Jersey, 1966.

[14] Tikhomolova, K.P., *Electro-Osmosis,* Ellis Horwood Ltd., Chichester, West Sussex, England, 1993.

[15] Smith, B.M., "Moisture Problems in Historic Masonry Walls," National Park Service, U.S. Department of the Interior, 1984.

[16] Hock, V.F., M. McInerney, and P. Malone, "Decision Paper - The Applicability of Electro-Osmotic Techniques for Preventing Water Seepage Through Porous Building Materials," U.S. Army Corps of Engineers – Engineer Research and Development Center, 1999.

[17] Hock, V.F., O.S. Marshall, M.K. McInerney, S. Morefield, P. Malone, C. Weiss, A.H. Kleinschmidt, K. Holtz, D. Goran, K. Richardson, and R. Condon, "Electro-Osmotic Pulse Technology for Control of Water Seepage in Various Civil Works Structures," ERDC TR-06-9, U.S. Army Corps of Engineers, Engineer Research and Development Center, 2006.

[18] McInerney, M.K., S. Morefield, S. Cooper, P. Malone, C. Weiss, M. Brady, J.P. Bushman, J. Taylor, and V. Hock, "Electro-Osmotic Pulse (EOP) Technology for Control of Water Seepage in Concrete Structures," ERDC/CERL TR-02-21, U.S. Army Corps of Engineers, Engineer Research and Development Center, Construction Engineering Research Laboratory, 2002.

[19] Morefield, S., V. Hock, M. McInerney, O. Marshall, C. Marsh, and S. Cooper, "Control of Water Migration Through Concrete Using Electro-Osmosis," Tri-Service Corrosion Conference, 2005.

[20] Hock, V.F., M.K. McInerney, and E. Kirstein, "Demonstration of Electro-Osmotic Pulse Technology for Groundwater Intrusion Control in Concrete Structures," FEAP Technical Report 98/68, U.S. Army Corps of Engineers, Construction Engineering Research Laboratory, 1998.

[21] Nemec, T.H., "Environmental pH Changes in Electrochemical Cell During Electro-Osmotic Stabilization of Soils," *Studia Geotechnica et Mechanica*, Vol. V, No. 1 (1983), 1988, pp. 13-38.

[22] Morefield, S.W., M.K. McInerney, V.F. Hock, O.S. Marshall, P.G. Malone, and C.A. Weiss, "Interface Modeling for Electro-Osmosis in Subgrade Structures," 24th Army Science Conference, Orlando, Florida, U.S. Army Corps of Engineers, Engineer Research and Development Center, 2005.

[23] Hock, V.F., M.K. McInerney, and E. Kirstein, "Demonstration of Electro-Osmotic Pulse Technology for Groundwater Intrusion Control in Concrete Structures," Tri-Service Corrosion Conference, 1997.

[24] Marshall, O.S., Personal communication, General EOP system figures and graphs, U.S. Army Corps of Engineers, Engineer Research and Development Center, Construction Engineering Research Laboratory, Champaign, Illinois, 2010-2011.

Appendix A

Examples of COE EOP Installations

Appendix A

Examples of COE EOP Installations

Electro-Osmotic Pulse (EOP) technology has been successfully installed in military structures such as family housing, steel reinforced deep structures, and tunnels. EOP has also been implemented on civilian structures such as residential structures, Washington DC Metro tunnels, and an underground treasury vault. EOP has been shown to prevent moisture seepage into below-grade structures. It is effective at keeping concrete surfaces at or below 50-percent humidity content, which keeps the treated space dry, the indoor relative humidity low, and prevents the growth of mold or mildew. This technology received the 2002 international NOVA award for innovation in construction, and it was twice nominated for the CERF Pankow award (1999 and 2004). The U.S. Army Corps of Engineers, Engineering Research and Development Center research on this technology has also been recognized by the 2004 Army Research and Development Achievement Award.
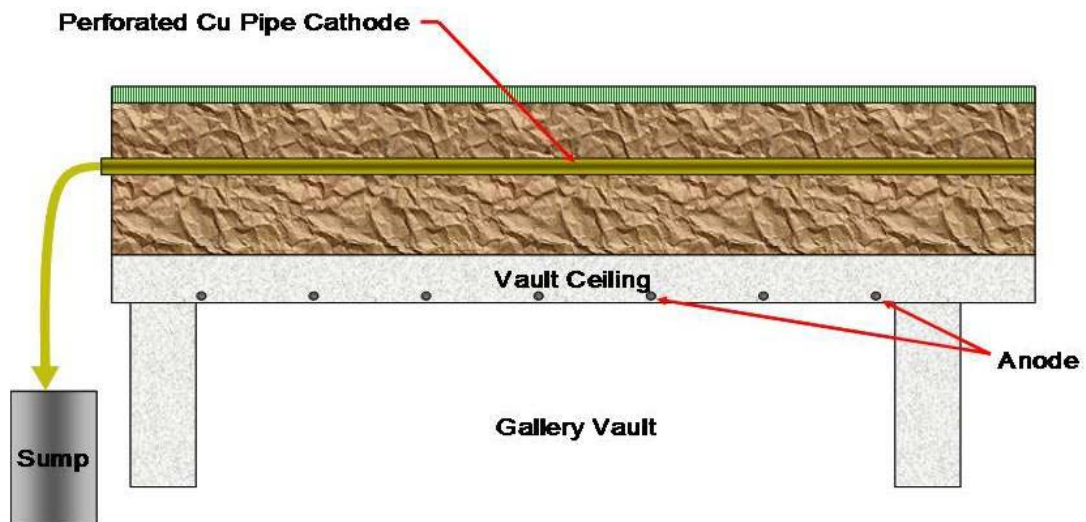
Lock and Dam No. 27 – Alton, Illinois

Before EOP   **After EOP**
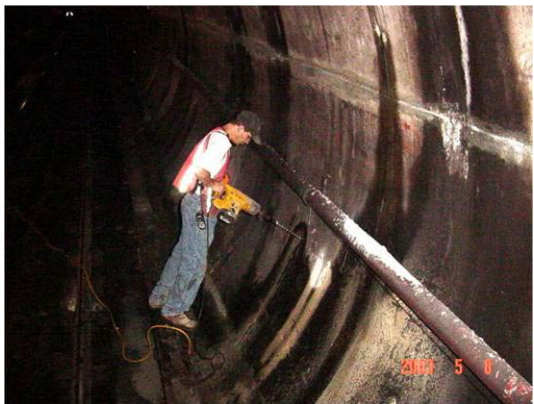
U.S. Treasury Building – Washington, DC

Before EOP   **After EOP**
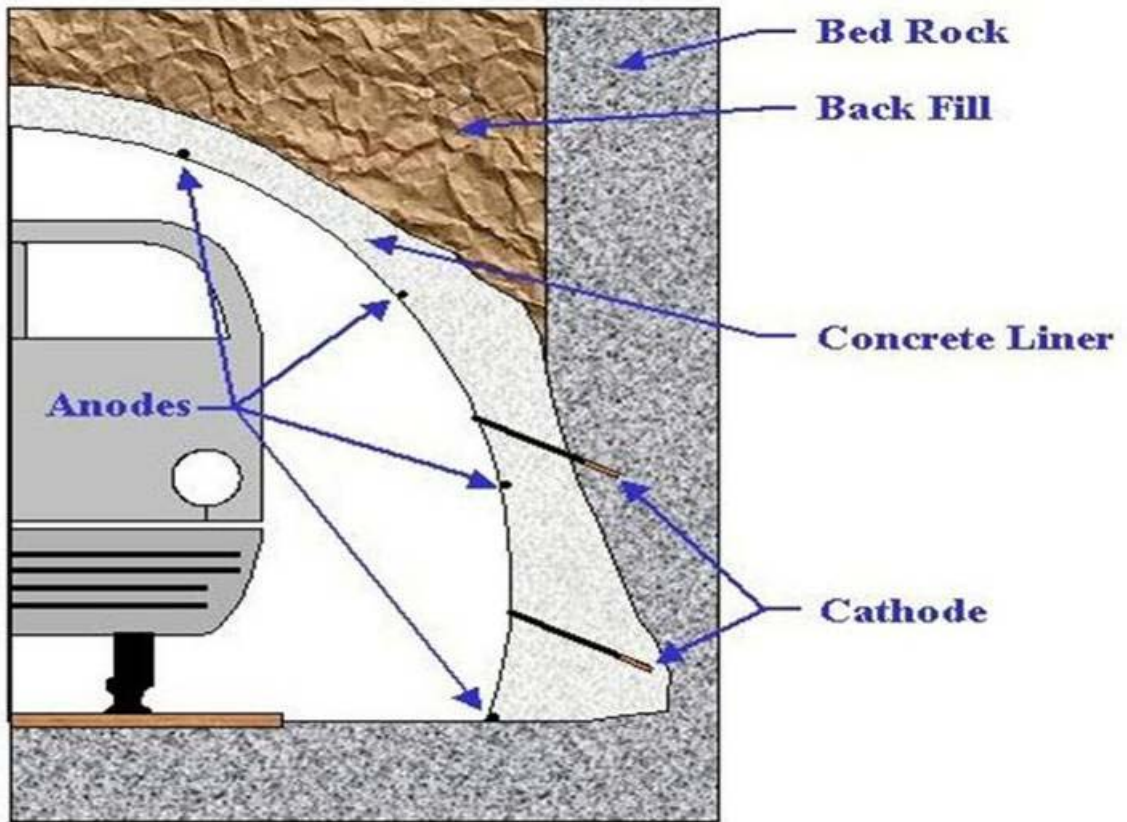

EOP design – direct drainage system
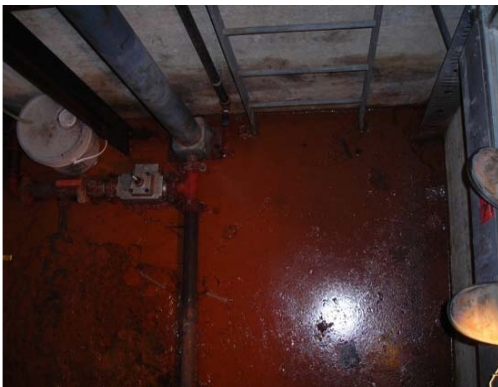
Metropolitan Tunnel – Washington, DC

Before EOP

After EOP

EOP design

Elevator Pit – Marsh's Edge, St. Simons Island, Georgia

Before EOP

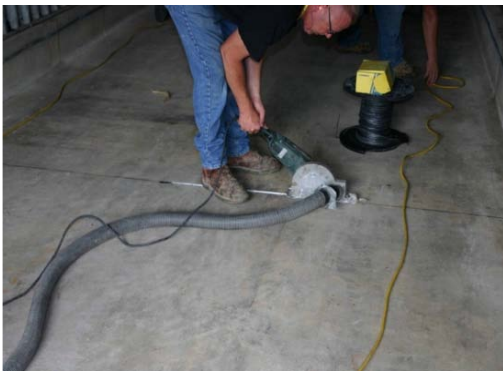
After EOP

Ammunition Bunker – Army Base, Eastern U.S.

Before EOP

Locating rebar in floor

Saw cutting grooves for cables

Chipping out groove for anode installation

Anode strips

Anode installation

Drilling hole for cathode

Installation of cathode rod

Exposed rebar

Rebar connection

Cable runs and grooves

Crack repair

Grouting embedded cables

Completed grouting of cables

Finished EOP system installation

System control unit